



Article

# Numerical Study on the Hydrodynamic Characteristics of Submarine Pipelines under the Impact of Real-World Tsunami-Like Waves

Enjin Zhao <sup>1,2</sup> , Ke Qu <sup>3</sup>, Lin Mu <sup>1,2,\*</sup>, Simon Kraatz <sup>4</sup>  and Bing Shi <sup>5</sup>

<sup>1</sup> College of Marine Science and Technology, China University of Geosciences, Wuhan 430074, China; zhaoej@cug.edu.cn

<sup>2</sup> Shenzhen Research Institute, China University of Geosciences, Shenzhen 518057, China

<sup>3</sup> School of Hydraulic Engineering, Changsha University of Science & Technology, Changsha 410114, China; kqu@csust.edu.cn

<sup>4</sup> Department of Civil and Environmental Engineering, University of New Hampshire, Durham, NH 03824, USA; Simon.Kraatz@unh.edu

<sup>5</sup> College of Engineering, Ocean University of China, Qingdao 266100, China; sediment@ouc.edu.cn

\* Correspondence: moulin1977@hotmail.com; Tel.: +86-027-67886151

Received: 26 December 2018; Accepted: 22 January 2019; Published: 29 January 2019



**Abstract:** Submarine pipelines have been extensively used for marine oil and gas extraction due to their high efficiency, safety, and low price. However, submarine pipelines are vulnerable to extreme waves (i.e., tsunami waves). Previous research has often used solitary waves as a basis for studying the impacts of tsunami waves on submarine pipelines, although the hydrodynamic characteristics and wave properties drastically differ from those of real-world tsunami waves. This paper numerically investigates the hydrodynamic characteristics of tsunami waves interacting with submarine pipelines, but instead uses an improved wave model to generate a tsunami-like wave that more closely resembles those encountered in the real-world. The tsunami-like wave generated based on a real-world tsunami wave profile recorded during a 2011 tsunami in Japan has been applied. Given the same wave height, simulation results show that peak hydrodynamic forces of the tsunami-like wave are greater than those of the solitary wave. Meanwhile, the duration of the acting force under the tsunami-like wave is much longer than that of the solitary wave. These findings underline the basic reasons for the destructive power of tsunamis. It is also noted that the hydrodynamic forces of the pipeline under the tsunami-like wave increase with wave height, but will decrease as water depth increases. In addition to the single pipeline, the complicated hydrodynamic characteristics of pipelines in tandem arrangement have been also numerically studied. It is believed that the findings drawn from this paper can enhance our understanding of the induced forces on submarine pipelines under extreme tsunami waves.

**Keywords:** n-wave; tsunami-like wave; solitary wave; submarine pipeline; hydrodynamic forces

## 1. Introduction

Submarine pipelines have been widely used for marine oil and gas extraction owing to their high efficiency, safety, and low price. Since many submarine pipelines are laid directly on the seabed in the real marine environment, they are vulnerable to damage caused by extreme waves, currents, and their joint actions. For instance, the submarine pipelines of the Pinghu oil and gas field in East China were damaged due to fatigue fractures under joint action of waves and currents in 2000. During the Hurricane Katrina (2005), 102 submarine pipelines in the Gulf of Mexico were significantly damaged [1]. Much research has been carried out with regards to protecting submarine pipelines from

devastating extreme surge and wave damage during their service periods. Tong et al. [2] presented a three-dimensional Large Eddy Simulation (LES) study on the hydrodynamics of a submarine pipeline located close to a wall impacted by current. Results showed that the drag coefficient on spanning sections of the pipeline is generally smaller than that of non-spanning sections, and due to the pressure gradient around the submarine pipeline, vortices shedding can be generated. The vortices shedding processes can cause the pipeline to vibrate [3,4]. Except for the influence of current on the pipeline, the hydrodynamic characteristics of a pipeline located near the seabed impacted by waves have also been investigated numerically or experimentally by many researchers. When the waves are irregular, those studies [5,6] showed that for the same conditions, the vibration amplitude of the pipeline impacted by an irregular wave is much larger than that of regular wave. An experimental investigation of wave impact loads on a slender horizontal cylinder has been conducted by Haley et al. [7] using a long wave flume. The results show that as the wave becomes very steep, the vector sum of the horizontal and vertical velocity components at the water surface may deviate significantly from the normal to the local water surface. Gao et al. [8] studied the wave forces on horizontal cylinder due to nonlinear focused wave groups and the secondary load cycle which occurs after the maximum wave crest passing the cylinder is observed. A numerical model was described by Chern et al. [9] that facilitates accurate predictions of the response behavior of a flexibly mounted horizontal cylinder under progressive waves. The model utilized a combination of direct forcing boundary simulation and the volume of fluid method to represent the moving body and water free surface. The results show that Reynolds number and Keulegan–Carpenter (KC) are two domination factors for the vibration of the submarine pipeline and the flow regime. Besides, Two-dimensional (2D) numerical simulations are performed to investigate free surface waves past two semi-submerged horizontal circular cylinders in tandem by Ong et al. [10]. When free surface waves pass two semi-submerged horizontal cylinders in tandem, for the cases with small spacing between the two cylinders, more prominent wave run-up and over-topping actions and larger positive force on upstream cylinder are observed as compared with that of the single cylinder case. According to the published articles, most studies considering submarine pipelines are conducted in general hydrodynamic conditions using experimental and numerical methods, such as steady uniform flow, airy wave, solitary wave, and so on. The intensities of forces impacting on the submarine pipelines under these conditions have been examined and analyzed, and the intensities are weaker than those under the tsunami wave.

In a real marine environment, extreme surges and waves induced by hurricanes or tsunamis can easily damage offshore and onshore infrastructures, especially submarine pipelines. To investigate the hydrodynamic characteristics of marine infrastructure subjected to tsunamis, the solitary wave has been widely used as the typical tsunami wave model since 1970s for numerical investigations [11–13] and experimental work [14–16]. For example, Francesco et al. [17] carried out the experimental and numerical investigations about the horizontal and vertical hydrodynamic forces induced by solitary waves on a horizontal circular cylinder placed on the half water depth. Small-scale laboratory tests have been performed in a wave flume and a diffusive weakly-compressible SPH model including a packing algorithm and a procedure was adopted. On the basis of the experimental and SPH results, the peaks and the shapes of the total wave forces in both directions are largely influenced by the inertia components in the present flow regime. Despite the widespread use of solitary wave, field observation, numerical simulation and experimental studies have shown that there are substantial differences between tsunami and solitary waves, such as wave profile and period [18]. Madsen et al. [19] pointed out that the required evolutionary distance for an initial free surface hump into a solitary wave far exceeds the width of any ocean on Earth and that real-world large-scale tsunamis would not evolve into solitary waves on geophysical scale. Based on the real-world tsunami profile recorded during the Tohoku tsunami event [20], tsunami waves were found to have significantly longer wavelengths than that of solitary waves. Qu et al. [21] carried out a detailed comparison between tsunami and solitary waves. It turned out that the tsunami wave produced a higher run-up distance than a solitary wave, making tsunami waves more dangerous and devastating.

Two other recent studies [22,23] investigated the tsunami induced forces on coastal structures via the use of both solitary waves and more realistic bores, and significant differences were revealed between the forces caused by two wave types. In particular, Leschka and Oumeraci [22] investigated the forces on three vertical cylinders with different distances and arrangements using a 3D RANS numerical model. The results showed that the two wave types introduce different wave heights in the vicinity of the cylinders and different magnitude and distribution of velocities. This in turn caused differences in the forces, which in the case of solitary waves were affected by the type of the cylinder arrangement and the distance between the cylinders, while in the case of bores, the forces were dominated by the arrangement type. Istrati et al. [23] presented a comprehensive analysis of data obtained during large-scale hydrodynamic experiments of tsunami waves impacting an I-girder bridge with cross-frames. The results showed that the bores introduced a short-duration impulsive horizontal force at the instant that the wave impacted the offshore girder, which always maximized the total horizontal force, followed by a force with smaller magnitude and longer duration as the wave flooded the chambers of the deck. However, this was not the case for solitary waves. Moreover, the study developed tsunami demand diagrams, which revealed significant differences in the patterns of horizontal and vertical forces, as well as the overturning moment between the unbroken solitary waves and bores. In general, previous research studies are indicating that the solitary wave is not a suitable wave model to study the hydrodynamic characteristics of tsunamis and their interaction with coastal infrastructure.

This paper numerically investigates the hydrodynamic characteristics of submarine pipelines impacted by tsunami waves using the real-world tsunami wave profile recorded at Iwate South station during Tohoku. The tsunami wave profile is approximated using a combination of three  $\text{sech}^2(*)$  wave profiles. The effects of prominent factors such as wave height, water depth, pipeline diameter, and gap-ratio on the hydrodynamic characteristics of submarine pipelines are discussed in detail. Hydrodynamic characteristics of pipelines in a tandem arrangement are also investigated. The paper is organized as follows: Section 2 describes governing equations and numerical methods; Section 3 describes the model validation; Section 4 presents the results and discussions; Section 5 summarizes the findings.

## 2. Numerical Model

### 2.1. Governing Equations

In the numerical simulation, the governing equations for incompressible flows are the three-dimensional Reynolds Averaged Navier–Stokes equations. The continuity equation in the vector form can be expressed as

$$\nabla \cdot \mathbf{U} = 0 \quad (1)$$

The momentum equation for incompressible flow can be written as

$$\frac{\partial \rho \mathbf{U}}{\partial t} + \nabla \cdot (\rho \mathbf{U} \mathbf{U}) = \nabla \mathbf{U} \cdot (\nabla \mu_e) + \nabla \cdot (\mu_e \nabla \mathbf{U}) - \nabla p + (\rho - \rho_r) \cdot \mathbf{g} \quad (2)$$

where  $\nabla$  is the gradient operator,  $\mathbf{U}$  is the flow velocity vector,  $\rho$  is the mixture density of air–water,  $t$  is the time,  $\mu_e$  is the effective viscosity,  $\rho_r$  is the reference density,  $p$  is the pressure, and  $\mathbf{g}$  is the gravity acceleration [24].

The  $k$ - $\omega$  model is used as the turbulence closure.

$$\frac{\partial}{\partial t}(\rho k) + \frac{\partial}{\partial x_i}(\rho k u_i) = \frac{\partial}{\partial x_j}(\Gamma_k \frac{\partial k}{\partial x_j}) + G_k - Y_k + S_k \quad (3)$$

$$\frac{\partial}{\partial t}(\rho \omega) + \frac{\partial}{\partial x_i}(\rho \omega u_i) = \frac{\partial}{\partial x_j}(\Gamma_\omega \frac{\partial \omega}{\partial x_j}) + G_\omega - Y_\omega + S_\omega \quad (4)$$

where  $\Gamma_k$  and  $\Gamma_\omega$  represent the effective diffusivity of  $k$  and  $\omega$ , respectively.  $G_k$  represents the generation of turbulence kinetic energy,  $G_\omega$  represents the generation of  $\omega$ ,  $Y_k$ , and  $Y_\omega$  represent the dissipation of  $k$  and  $\omega$ ,  $S_k$  and  $S_\omega$  are source terms. In the simulation, the  $k$ - $\omega$  model is used as the turbulence closure due to two reasons. Firstly, the simulation and calculation of the fluid nearby the wall are more stable using this turbulence model than other models. In order to capture the detailed flow around the wall of submarine pipeline, this turbulent closure is selected. Secondly, the calculation accuracy of the model can be ensured when the counter-pressure gradient flow is simulated. So, this turbulent closure is suitable for the solution of free shear turbulence flow, boundary layer turbulence flow, and moderate separation turbulence flow when the wave passes the submarine pipeline.

In the model, the transportation equation of the volume of fluid (VOF) method is written as

$$\frac{\partial \gamma}{\partial t} + \nabla \cdot (\gamma \mathbf{U}) = 0 \tag{5}$$

The local density and laminar viscosity of every mesh grid are defined by volume fraction  $\gamma$ , which is adopted to capture the free surface between water and air for the generation and propagation of wave.

$$\rho = \rho_{air} + \gamma \cdot (\rho_{water} - \rho_{air}) \tag{6}$$

$$\mu_l = \mu_{air} + \gamma \cdot (\mu_{water} - \mu_{air}) \tag{7}$$

$$\gamma = \begin{cases} \gamma = 0 & , \quad air \\ 0 < \gamma < 1 & , \quad interface \\ \gamma = 1 & , \quad water \end{cases} \tag{8}$$

In the model, the collocated finite volume method is implemented to discretize the continuity and momentum equations, and the deferred correction is employed to discretize the convective terms by combining the first-order upwind scheme and the second-order Gamma scheme. In order to couple the continuity and momentum equations, the momentum interpolation method is adopted to interpolate the velocities of the control cell centers to the control cell faces [25]. And then the velocities and pressures are resolved by the Pressure Implicit Split Operator (PISO) method. The sharpness of the free surface between the water and air is controlled by the Switching Technique for Advection and Capturing of Surfaces (STACS).

### 2.2. Wave Generation Method

A piston-type wave maker is simulated using the dynamic mesh technology, as shown in Figure 1. In hexahedral mesh zone, the layer height ( $H_l$ ) is specified on moving boundary firstly. Based on the height, the layer of cells (layer  $j$ ) adjacent to the moving boundary is split or merged with the layer of cells (layer  $i$ ) next to it. The dynamic layering mesh adjacent to moving boundary is added or removed layers of cells. To produce the desired free surface profile, the position of the moving boundary changes with time [26,27]. Solitary and tsunami waves are generated using the piston-type wave maker depending on the following methods.

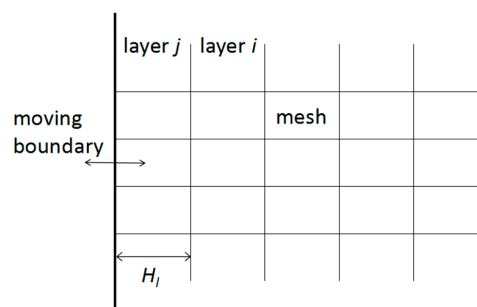


Figure 1. Dynamic layers of moving boundary.

The wave elevation of the solitary wave with a constant water depth  $h$  can be written as

$$\eta(x_i, t) = H_o \operatorname{sech}^2[k_o(x - x_o - C_o T_o)] \tag{9}$$

where  $H_o$  is the wave height,  $k_o = (3H_o/4h^3)^{1/2}$  is the effective wave number,  $x_o$  is the location of the wave crest at  $t = 0$ ,  $C_o = [g(H_o + h)]^{1/2}$  represents the wave celerity,  $T_o$  is the wave period of a solitary wave which is defined by the effective wave number.

To reproduce the real-world tsunami wave, a combination of three  $\operatorname{sech}^2(*)$  wave profiles is used to model the tsunami wave based on the concept of N-wave. The combination of three  $\operatorname{sech}^2(*)$  wave can be written as

$$\eta(x_i, t) = \sum_{i=1}^3 H_i \operatorname{sech}^2[\omega_i(t - (t_o + t_i))] \tag{10}$$

In the following sections, we name the wave profile described by Equation (10) as tsunami-like wave. To enable a general application of tsunami-like wave profile, the parameters of the tsunami-like wave presented in previous researchers [20,28] have been normalized as follows

$$\begin{aligned} \left( \frac{H_1}{H_o} \quad \frac{\omega_1}{\omega_o} \quad \frac{t_1}{T_o} \right) &= \left( -0.119 \quad 0.0856 \quad 6.556 \right) \\ \left( \frac{H_2}{H_o} \quad \frac{\omega_2}{\omega_o} \quad \frac{t_2}{T_o} \right) &= \left( 0.328 \quad 0.0947 \quad 8.776 \right) \\ \left( \frac{H_3}{H_o} \quad \frac{\omega_3}{\omega_o} \quad \frac{t_3}{T_o} \right) &= \left( 0.873 \quad 0.31244 \quad 10.54 \right) \end{aligned} \tag{11}$$

where  $\omega_o$  is the wave frequency of a solitary wave with the same wave height as the tsunami-like wave.

To generate solitary wave and tsunami-like wave, the velocity of wave paddle can be described as

$$u = \sum_{i=1}^3 u_i \tag{12}$$

and

$$u_i = C_i \eta_i / (h + \eta_i) \tag{13}$$

The wave profile approximated by the wave generation formula and the observed wave profile at Iwate South station during 2011 Japan tsunami event are shown in Figure 2.

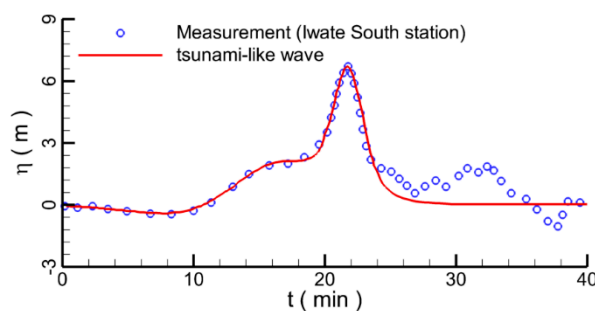


Figure 2. Comparison between the tsunami-like wave and the measured wave.

### 3. Model Validation

To evaluate the computational capability of our model in predicting hydrodynamic forces, solitary wave impacting the submarine pipeline is numerically investigated in this section. The corresponding experimental work was performed by Sibley [29]. The experimental layout is shown in Figure 3, where  $D$  is the pipe diameter and  $G$  is the space between the pipe and the bottom boundary. The wave height and water depth are denoted as  $H$  and  $h$ , respectively.

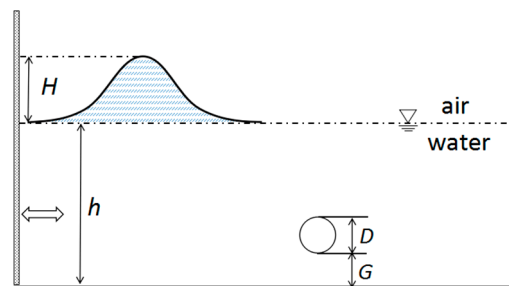


Figure 3. Schematic representation of the experimental layout.

Two experimental runs are selected using parameters provided in Table 1. The computational domain is 30 m in length and 0.5 m in height. The origin of the  $x$  coordinate is set at the left boundary and the origin of the  $z$  coordinate is set at the bottom boundary. The center of the circular cylinder is located at  $x = 3$  m. The computational mesh consists of 365,512 elements and the mesh resolution near the circular cylinder is about 0.05 mm. To meet the mesh resolution requirement, another two groups of meshes have been generated: a medium and coarse mesh with 185,145 and 91,497 mesh elements, respectively.

Table 1. Parameters of selected experimental runs.

Run	$h$ (m)	$H$ (m)	$D$ (m)	$G$ (m)
1	0.17	0.034	0.034	0.0714
2	0.16875	0.03105	0.027	0.023625

Figure 4 depicts the snapshots of the vorticity contour at different times for run 1. When the solitary wave approaches the cylinder, a pair of vortices are gradually generated at the rear side of the cylinder. Once the solitary wave passes over cylinder, vortices can be shed from the cylinder surface and complicated flow phenomena can be observed (Figure 4d). Figure 5 depicts the snapshots of the vorticity contour for run 2. When the crest of the solitary wave is above the pipeline, a pair of narrow vortices are formed behind the pipeline. After vortices are shed from the cylinder, they strongly interact with the boundary layer at the seabed (Figure 5d).

Time series comparisons of the resultant hydrodynamic forces at the pipeline between measurements and numerical predictions are plotted in Figure 6 (run 1) and Figure 7 (run 2), where both horizontal and vertical forces are nondimensionalized by  $\rho ghA$  ( $A = \pi D^2/4$ ), namely,  $F^* = F/\rho ghA$ . In the rest of the paper, all hydrodynamic forces are presented using this method. Predicted horizontal and vertical forces are in good agreement with corresponding measurements in both peak force values and temporal evolution process. Forces for the medium and dense meshes are nearly identical whereas those computed on the coarse mesh are noticeably different from measurement. Hence, the resolution of dense mesh and medium mesh is sufficient. In order to guarantee the calculation accuracy, a similar resolution mesh setup as dense mesh will be applied in the following simulation. By carrying out the simulation work in this section, the computational capability of our model in predicting the hydrodynamic forces of submarine pipeline is well calibrated.

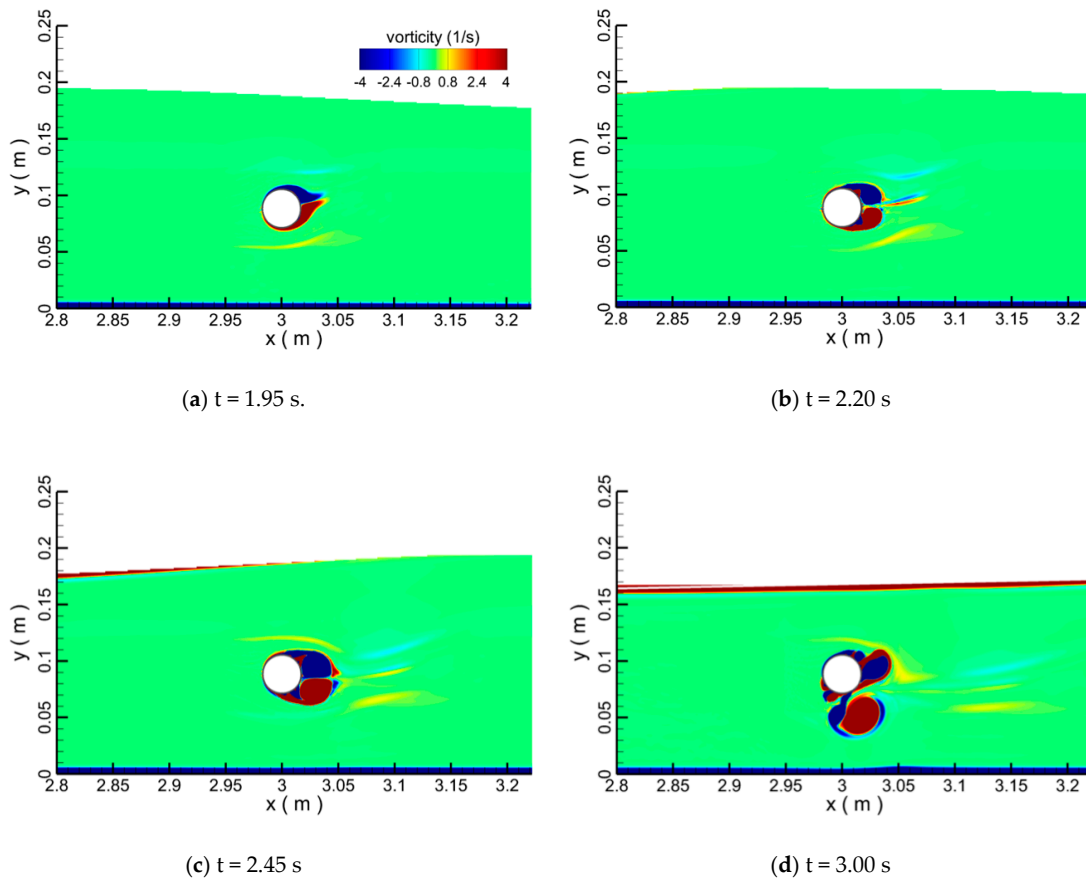


Figure 4. Snapshots of vorticity contour of the flow field at different times for run 1.

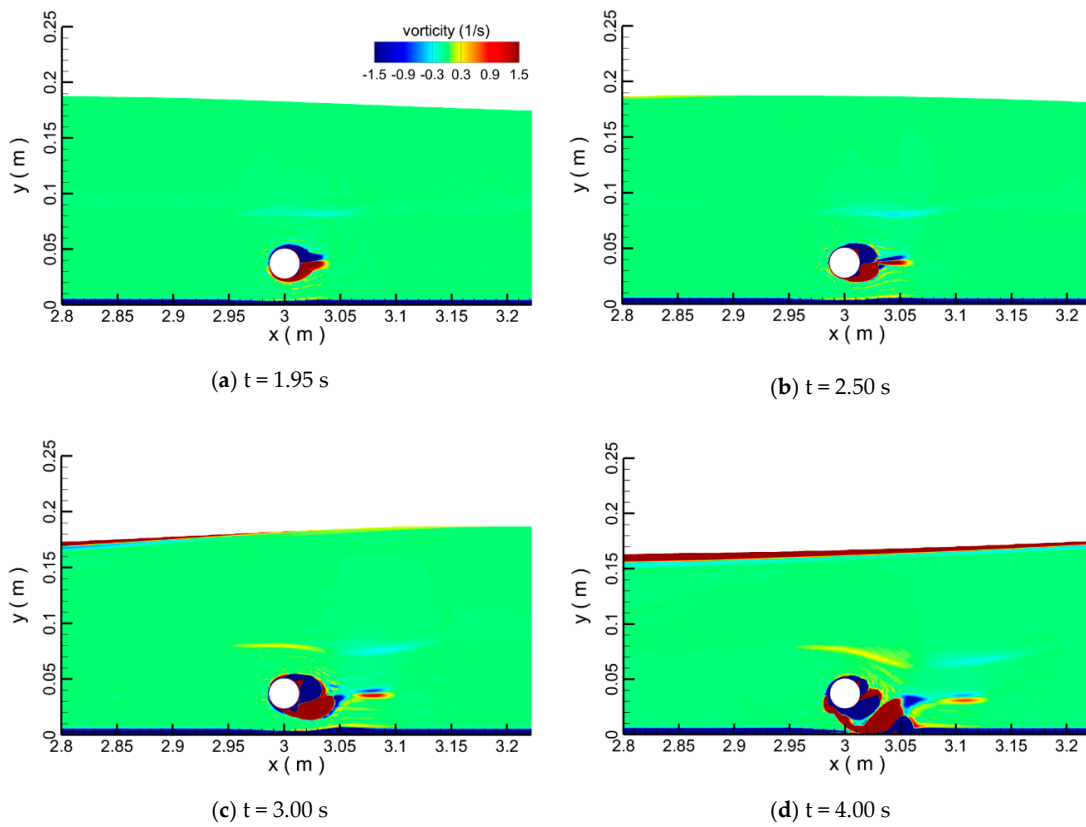
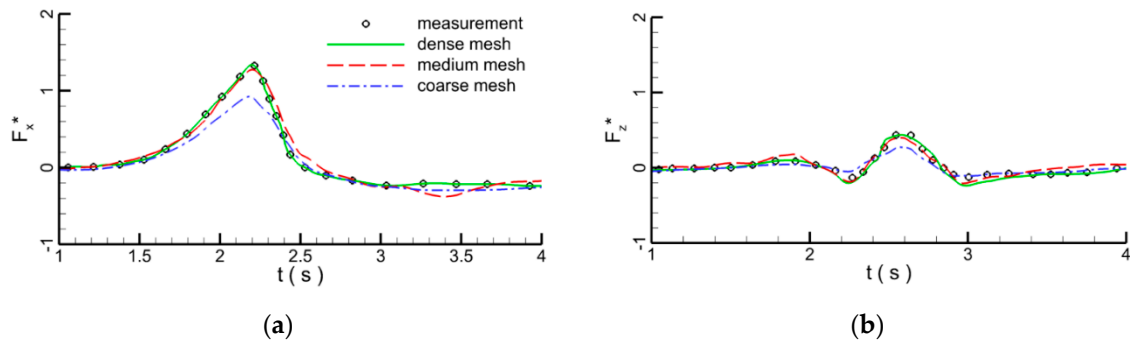
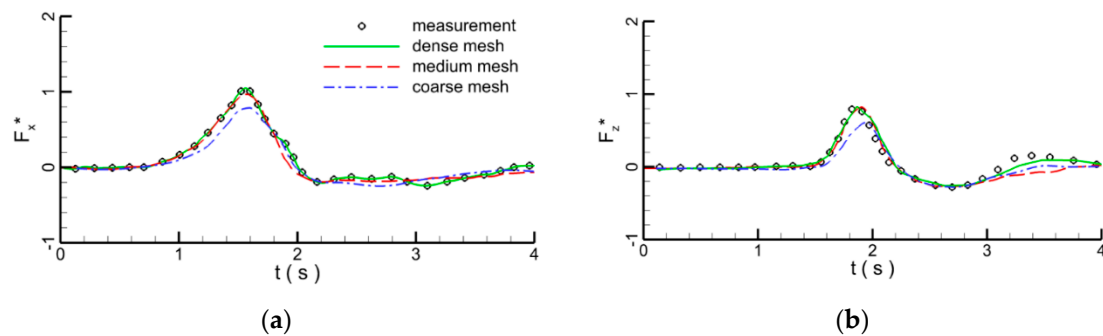


Figure 5. Same as Figure 3 but for run 2.



**Figure 6.** Force comparison between measurement and simulation in run1; (a) horizontal force  $F_x^*$ ; (b) vertical force  $F_z^*$ .



**Figure 7.** Force comparison between measurement and simulation in run 2; (a) horizontal force  $F_x^*$ ; (b) vertical force  $F_z^*$ .

#### 4. Results and Discussions

The hydrodynamic characteristics of submarine pipelines impacted by the tsunami-like wave are systematically investigated. Effects of prominent factors, such as wave height, water depth, pipeline diameter, and spacing distance between pipeline and seabed are discussed in detail. For comparison purpose, the flow field around pipelines under solitary wave conditions is also numerically simulated. In ocean engineering, many pipelines transport gas and oil in tandem, so the hydrodynamic environment around a tandem pipeline is also investigated. In this study, the marine environmental conditions are referred to the Bohai Sea in China which is the innermost gulf of the Yellow Sea and the Korea Bay on the coast of Northeastern and North of China. Many submarine pipelines are working in the Suizhong 36-1 Oil Field which is located in Liaodong Bay of Bohai Sea and the distance from this oilfield to Suizhong County is about 50 km. The sea area is relatively flat and there are not many steep slopes. Considering the marine environmental conditions in this realistic oil field, the parameters of this study are selected.

The computational domain is 2000 m in length and 20 m in height. The horizontal coordinate of the pipeline center is  $x = 100$  m. The mesh resolution around the submarine pipeline is similar to that presented in Section 3. In the whole computational domain, the mixed grids are adopted where unstructured grids are around the submarine pipeline with the grid size of 0.05 m and structured grids are used in another domain. When the wave passes the pipeline, the effect of the wave on submarine pipeline becomes weaker and weaker and the mesh behind the submarine pipeline also becomes looser and looser. The scale of grid increases depending on the increase ratio of 1.2. In the whole computational domain, about 956,000 grids are used. The computational layout of the single pipeline is depicted in Figure 8, where P is the velocity sensor locating at ( $x = 50$  m,  $z = 1$  m), and L1 and L2 are the elevation sensors locating at  $x_1 = 100 - 0.55D$  m and  $x_2 = 100 + 0.55D$  m, respectively. The computational layout for the pipelines in tandem arrangement is shown in Figure 9, where S is the distance between two pipelines. The time-step size is 0.005 s, the number of time steps are  $10^5$  and the maximum iterations are 20. Depending on the numerical model, 2D simulations are conducted.



The calculation was performed on the a Dell Precision 3630 Tower, which includes 12 central processing units (CUPs). The CPU type is Intel (R) Core (TM) i7-8700 CUP @ 3.20GHz which is produced by Intel Corporation, California, America. The storage of the internal memory and hardware are 16G and 2T, respectively. In order to save computation time, four cases were run simultaneously on one computer. The real duration for one case is about 115 h. When the simulation begins, the program reads the initial boundary conditions and mesh grids. Depending on the numerical methods, the results are generated and saved according to the storage time step. Because the moving-mesh method is used in the simulation, when the results are saved, the changed meshes are also saved.

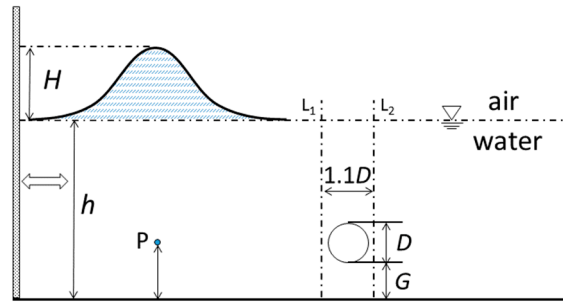


Figure 8. Computational layout for wave impacting a single submarine pipeline.

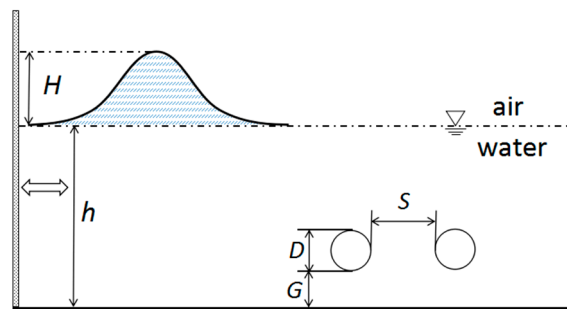


Figure 9. Computational layout for wave impacting pipelines in tandem arrangement.

#### 4.1. Single Pipeline

In this section, a tsunami-like wave impacting single pipeline is numerically investigated. The water depth  $h$  and wave height  $H$  are 8 m and 2 m, respectively. The pipeline diameter  $D$  is 1 m and the pipeline is located on the seabed ( $G = 0$ ). In the study, the submarine pipeline is laid on the seabed directly without any gap and we did not consider the gap ratio in this case. The flow cannot pass at the bottom of the submarine pipeline. The surface of the submarine pipeline connects the seawall, as shown in the small graph of Figure 10. The distance between the start point and the end point is about 0.02 m which is much less than the pipeline diameter of 1 m. Also, the contact between the submarine pipeline and seabed is more realistic in ocean engineering. As for the forces, we integrated the forces distributed on the whole cylinder from the start point to the end point.

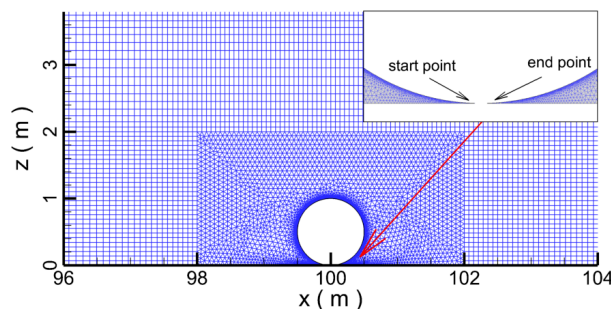
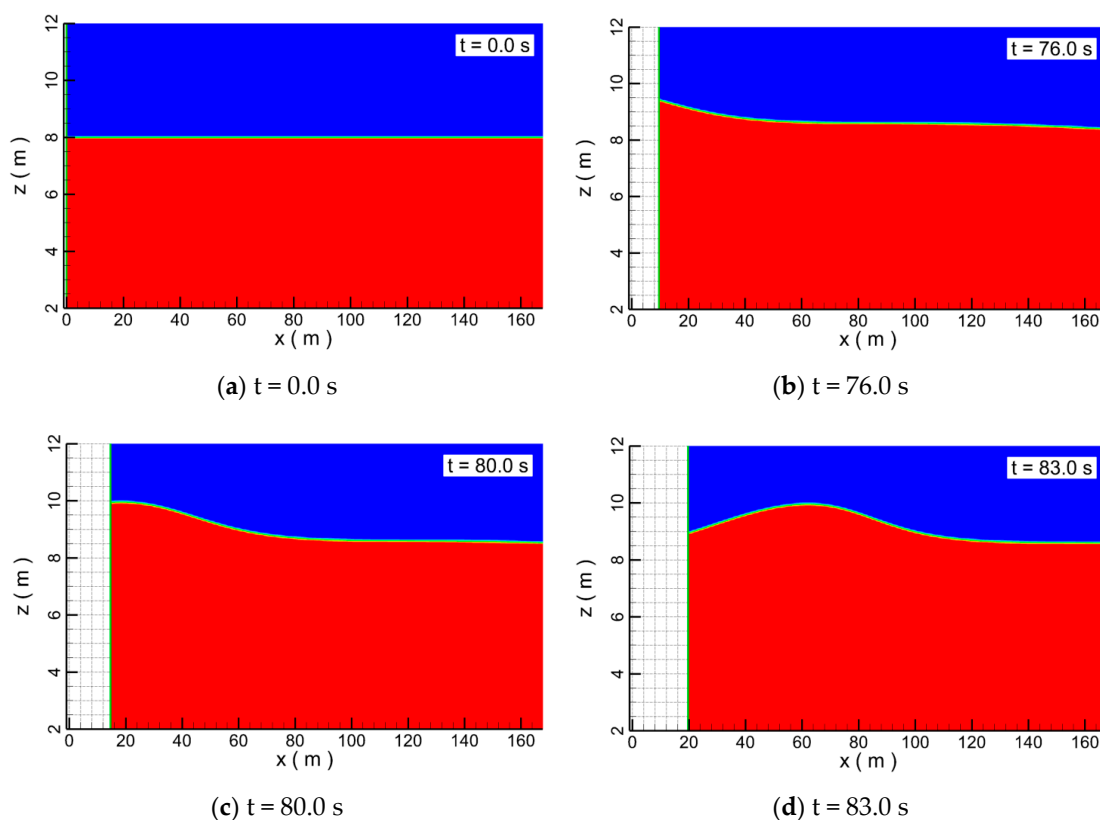


Figure 10. The mesh setup around the submarine pipeline.

In Figure 11, due to the movement of the boundary from the left to right, the water is compressed and the water level rises, which generates the wave. At the beginning of wave generation, the wave generation paddle is placed at  $x = 0$ , and the surface of the water remains horizontal. At 76 s, the numerical wave generation paddle moves along the  $x$  axis, pushing the water and generating the wave. At 80 s, the crest of the tsunami-like wave is created by the wave generation paddle. The shape of the tsunami-like wave can be seen in Figure 11d. The results suggest that when the boundary moves, the wave is generated and propagates steadily along the flume (Figure 11), which means this wave-making method can generate a satisfactory wave for the research.



**Figure 11.** The wave generation process around the wave paddle.

The profiles of the tsunami-like wave and the solitary wave generated by the piston-type wave maker are displayed in Figures 12a and 13a.

Three parts of the tsunami-like wave can be seen:

- (1) the leading-depression wave portion;
- (2) the preceding elevated wave portion;
- (3) the secondary elevated wave portion.

Compared with the solitary wave (Figure 13a), the duration of the tsunami-like wave is much longer (Figure 10a). As the crest of the tsunami-like wave approaches the pipeline, small vortices are gradually generated at the frontal and rear sides of pipelines (Figure 12). At  $t = 136$  s, when the crest of the wave is just above the pipeline, the velocity magnitude of the flow field around the pipeline approaches its maximum and the free surface above the pipeline is rather flat (Figure 12b). After the tsunami-like wave passes the pipeline, the size of the vortices at the frontal and rear sides of pipeline increases substantially, even though the magnitude of the flow velocity near the pipeline decreases (Figure 12c). There are two main regions where the magnitude of the velocity is large when the crest of the solitary wave is located above the pipeline: the region just above the pipeline, and the region near the water surface (Figure 13b). Besides, the water free surface under the tsunami-like wave is gentler

than that under the solitary wave, because the duration of the tsunami-like wave is longer than that of solitary wave. After the solitary wave has passed the pipeline, the vortices behind the pipeline are much smaller than for the tsunami-like wave (Figures 12c and 13c).

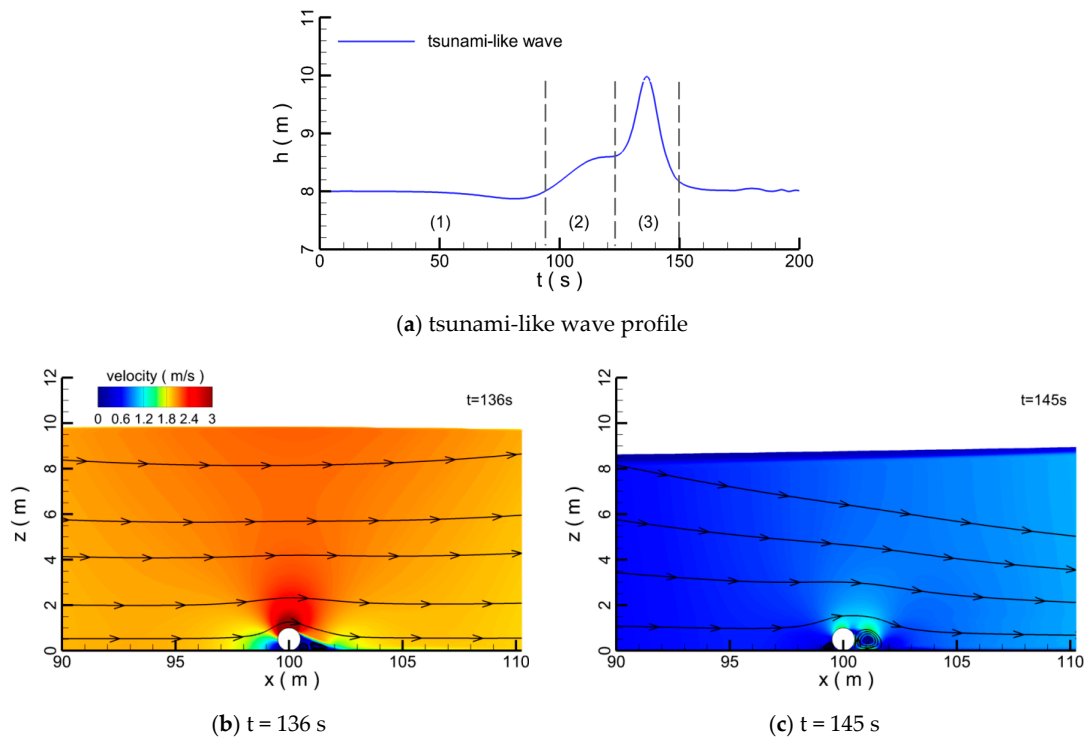


**Figure 12.** Snapshots of the velocity contour around the submarine pipeline at different times for the tsunami-like wave.

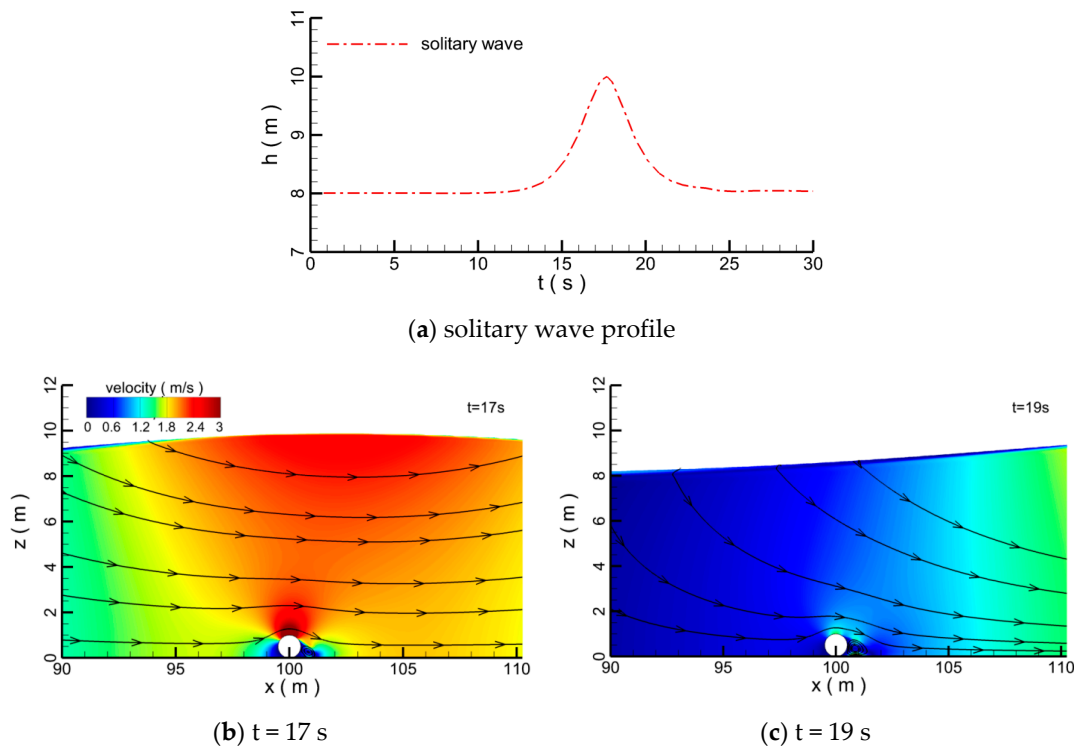


**Figure 13.** Snapshots of the velocity contour around submarine pipeline at different times for the solitary wave.

Time series of water elevation recorded at elevation sensors  $L_1$  and  $L_2$  under tsunami-like wave and solitary wave conditions are depicted in Figure 14. Since the diameter of the pipeline is relatively small compared to still water depth, for both solitary and tsunami-like waves, the wave profiles are almost unchanged. Although the blocking effect of the pipeline on wave propagation is very weak, the crests of two waves still fluctuate slightly. The wave heights decrease for both waves when they pass through the pipeline. The wave height of the solitary wave decreases more than that of the tsunami-like wave. The difference between the two wave shapes are independent of the difference in the wave peaks due to the different scattering. The maximum velocity of the tsunami-like wave measured at P is about 1.15 times of that of the solitary wave at the same wave height (Figure 15). Also, the duration of the high-velocity portion is much longer for the tsunami-like wave.

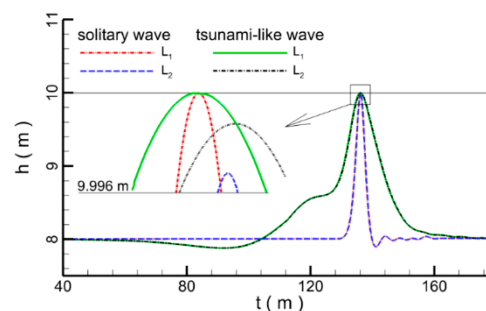


**Figure 14.** Time series of water elevations recorded at elevation sensors  $L_1$  and  $L_2$  for the solitary and tsunami-like wave.

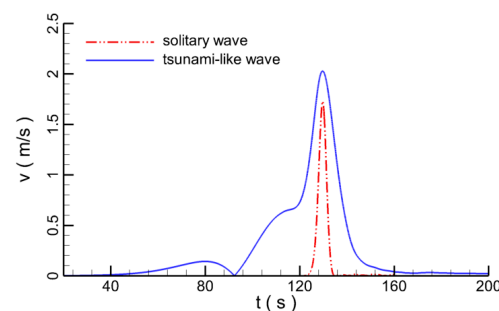


**Figure 15.** Time series of velocity at velocity sensor P during the tsunami-like wave and solitary wave.

The time series of the horizontal and vertical forces exerted at the pipeline when impacted by the tsunami-like and solitary waves are plotted in Figure 16. The horizontal and vertical forces on the cylinder are obtained from surface integration of the hydrostatic pressure, hydrodynamic pressure, and shear stresses. When the flow arrives at the submarine pipeline, due to the obstruction of the pipeline to the water body, the flow velocity reduces and flow direction changes. Correspondingly, the submarine pipeline suffers the force of the flow. The peak values of the horizontal and vertical forces for the tsunami-like wave are larger than for the solitary wave. The horizontal force peaks for both waves are similar to each other; on the contrary, noticeable differences can be detected in the vertical forces, which are caused by two reasons. Firstly, when the wave passes the pipeline, the velocity of the tsunami-like wave is larger than that of the solitary wave. The bottom water flows from the seabed to the top of the submarine pipeline, which is mainly subjected to vertical upward force. The larger the velocity, the larger the vertical upward force. Secondly, the crest levels for two different waves are different after the waves pass through the pipeline. The vertical force includes the vertical hydrodynamic force and the hydrostatic force. The crest level of the tsunami-like wave is higher than that of the solitary wave, which also causes the vertical force under the tsunami-like wave to be larger than that of the solitary wave. However, the horizontal force only includes the hydrodynamic force which is affected by the horizontal velocity. Due to the fact that the horizontal velocities of two waves are similar to each other, the horizontal force peaks under two waves are also

close. Interestingly, in the horizontal direction, the negative force also can be seen in Figure 16a. It is very easy to understand that when the wave passes the submarine pipeline, the horizontal flow causes the force on the submarine pipeline in normal direction due to the pressure gradient in front and to the rear of the submarine pipeline. The greater the velocity, the greater the force. However, after the wave passes the submarine pipeline, the pressure gradient does not disappear rapidly. Much water will flow to the negative pressure zone behind the submarine pipeline, which causes the water reflux. The reflux water will induce flow in the negative direction. When the negative flow acts on the submarine pipeline, negative horizontal force is generated. This is a normal phenomenon in the wave propagation for the tsunami-like and solitary wave. The pressure gradient caused by the wave determines the velocity of the water reflux. The larger the pressure gradient, the more the reflux water and the greater the negative horizontal force on the submarine pipeline. Due to the interaction between the submarine pipeline and flow, the energy contained by the flow dissipates gradually, the pressure gradient reduces, and the water finally reaches the equilibrium state. The horizontal force on the submarine pipeline reduces to zero. In general, the duration of the tsunami-like wave is longer than that of solitary wave. The duration of the acting force under the tsunami-like wave is also much longer than for the solitary wave, and the more energy is contained by the tsunami-like wave. Under the action of a tsunami-like wave, the pipeline is more like to be damaged. The presented results show that a real-world tsunami wave cannot be directly simplified to a solitary wave, and explains the reasons for the devastating power of tsunami waves due to their large impact intensity and longer duration.

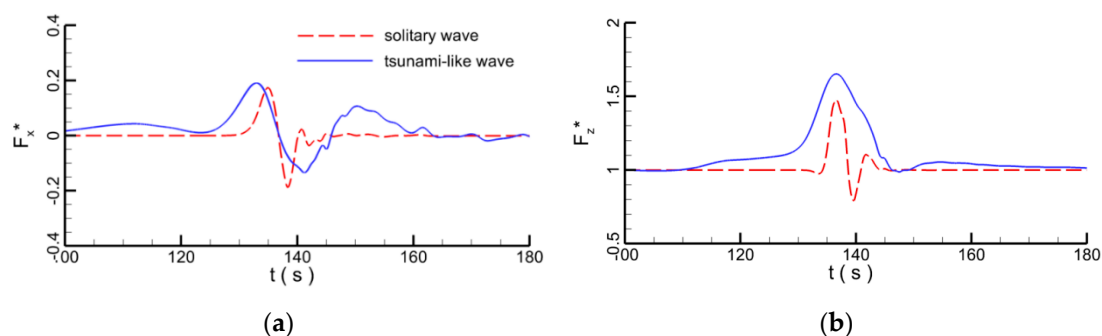


**Figure 16.** Time series of hydrodynamic forces at a pipeline under tsunami-like and solitary waves; (a) horizontal force  $F_x^*$ ; (b) vertical force  $F_z^*$ .

Based on the above research, the effects of wave height, water depth, pipeline diameter, and spacing between pipeline and seabed are discussed.

#### 4.1.1. Effect of Water Depth

This section discusses the impact of water depth on the hydrodynamic characteristics of the submarine pipeline. With a wave height  $H = 2$  m, pipeline diameter  $D = 1$  m, and  $G = 0$ , six different water depths are selected: 4 m, 6 m, 8 m, 10 m, 12 m, and 14 m. For comparison purposes, the time series of water elevation recorded at elevation sensor  $L_1$  at different water depths are plotted in Figure 17. It is seen that the wave profile of the tsunami-like wave gradually becomes fatter and its wave period becomes longer as water depth increases, thus increasing its energy carrying capacity.

The time series of flow velocity magnitude recorded at velocity sensor P during tsunami-like wave impacting the pipeline are displayed in Figure 18. When the water depth increases (Figure 18a), the maximum velocity decreases (Figure 18b). For example, when the water depth is 4 m, the maximum velocity magnitude is about 2.7 m/s, however, when the water depth is 14 m, the velocity decreases to 1.5 m/s.

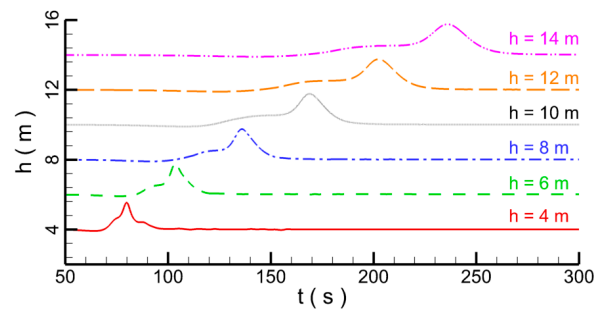


**Figure 17.** Time series of water elevation recorded at elevation sensor  $L_1$  for a tsunami-like wave at different water depths.

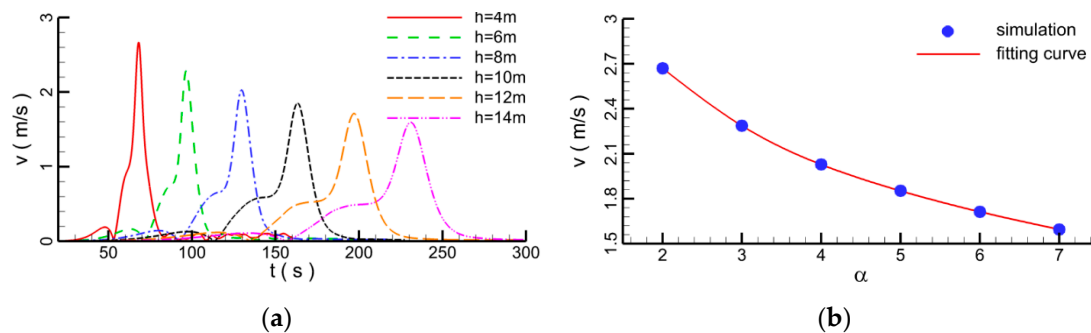


**Figure 18.** The variations of velocity at different water depths recorded at sensor P; (a) time series of velocity; (b) maximum velocity as function of water depth.  $\alpha$  is the ratio of water depth  $h$  to the wave height  $H$ .

The maximums and minimums of horizontal and vertical forces as functions of water depth for the solitary and tsunami-like waves are shown in Figure 19. Interestingly, as water depth increases, both maximum horizontal and vertical forces decrease (Figure 19a,b), and the magnitude of the minimum forces decreases at the same time (Figure 19c,d). This is consistent with the variations of velocity shown in Figure 18 as water depth increases, inflow velocity in front of the pipeline decreases, and hence the resultant hydrodynamic forces also decrease. When the water depth is greater than 6 m, the maximum horizontal forces of the solitary wave and tsunami-like wave become similar. With the increase of water depth, the shoaling becomes weaker and weaker. This is the main reason why the tsunami wave is not obvious in the deep sea, but in shallow water around a beach, a tsunami-wave can cause the tremendous damage. Similarly, with the increase of water depth, the difference of maximum forces on the submarine pipeline under the tsunami wave and solitary wave becomes smaller and smaller. However, the solitary wave still cannot be used instead of a tsunami-like wave to study the effect of tsunami waves on ocean or coastal infrastructure. In some special conditions, the maximum forces under two different wave types are similar, but not the same. The duration of the acting force under the tsunami-like wave is also much longer than for the solitary wave. In other words, the energy contained by the tsunami-like wave is much greater than that of a solitary wave. Besides, the changes of the forces on the submarine pipeline under two types of wave are also completely different, which may cause the different fatigue damage to the pipelines. However, for the same wave height and water depth, the maximum hydrodynamic forces at the pipeline under solitary wave are always smaller than that of tsunami-like wave. There is a great difference between maximum force and minimum force for tsunami-like wave and solitary wave. This is because when the waves pass the submarine pipeline, the maximum force is caused by the horizontal velocity which is similar for the two different types of wave. However, the minimum force is caused by the water reflux after the wave passes the submarine pipeline. The pressure gradient around the pipeline and water volume under the tsunami-like wave are much greater than that of a solitary wave, so the effect of the water reflux under

the tsunami-like wave is more serious than for a solitary wave. Compared with the maximum forces under the tsunami-like wave and solitary wave, the minimum forces are more different.

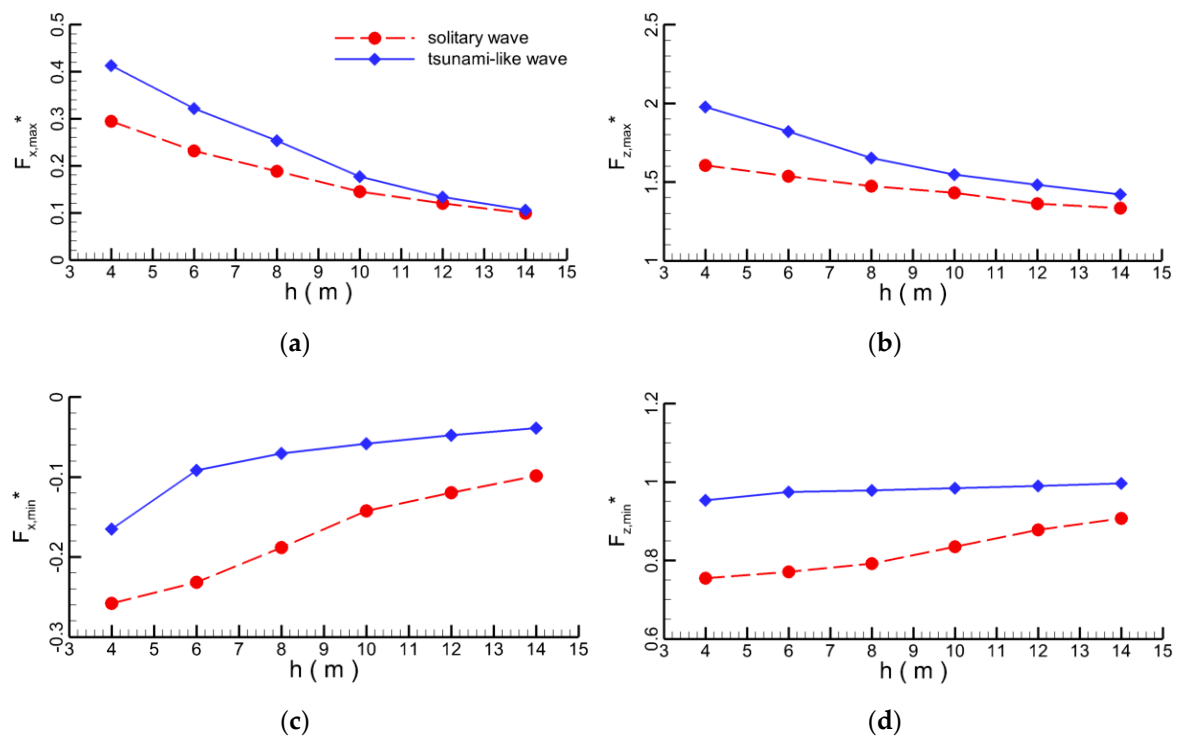


**Figure 19.** Plots of maximum forces as function of water depth; (a) maximum horizontal force  $F_{x,max}^*$ ; (b) maximum vertical force  $F_{z,max}^*$ ; (c) minimum horizontal force  $F_{x,min}^*$ ; (d) minimum vertical force  $F_{z,min}^*$ .

#### 4.1.2. Effect of Wave Height

This section numerically investigates the effect of wave height on the hydrodynamic forces at the pipeline for the tsunami-like wave. The water depth  $h$  is 10 m, the pipeline diameter  $D$  is 1 m, and it is located at the seabed ( $G = 0$ ). Four different wave heights are selected:  $H = 1$  m, 2 m, 3 m, and 4 m. The duration is largely decreasing with increasing wave height (Figure 20). The maximum velocity recorded at sensor P increases monotonically with wave height (Figure 21).

Both the maximum horizontal and vertical forces gradually increase with wave height (Figure 22a,b), but much more rapidly for the tsunami-like wave. This again demonstrates that the hydrodynamic characteristics of the tsunami-like wave are drastically different from that of the solitary wave. As the wave height increases, the magnitudes of the minimum horizontal and vertical forces gradually decrease (Figure 22c,d).

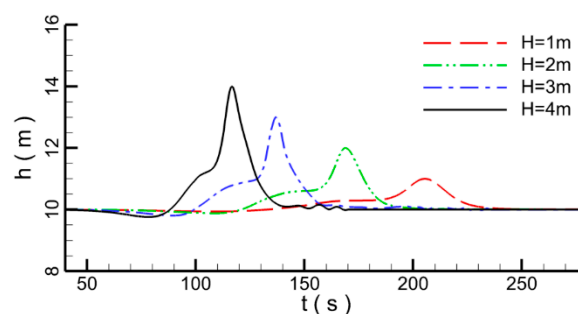


**Figure 20.** Time series of the tsunami-like wave profile recorded at sensor  $L_1$ .

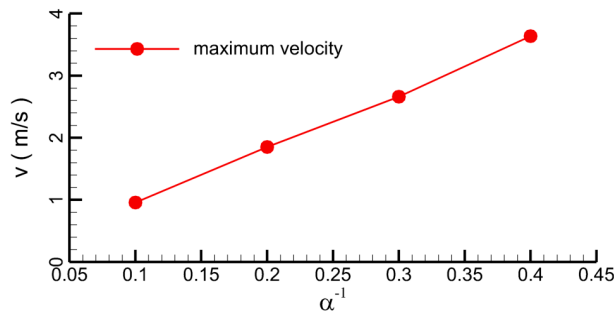


Figure 21. Plots of maximum velocity recorded at sensor P as function of wave height.

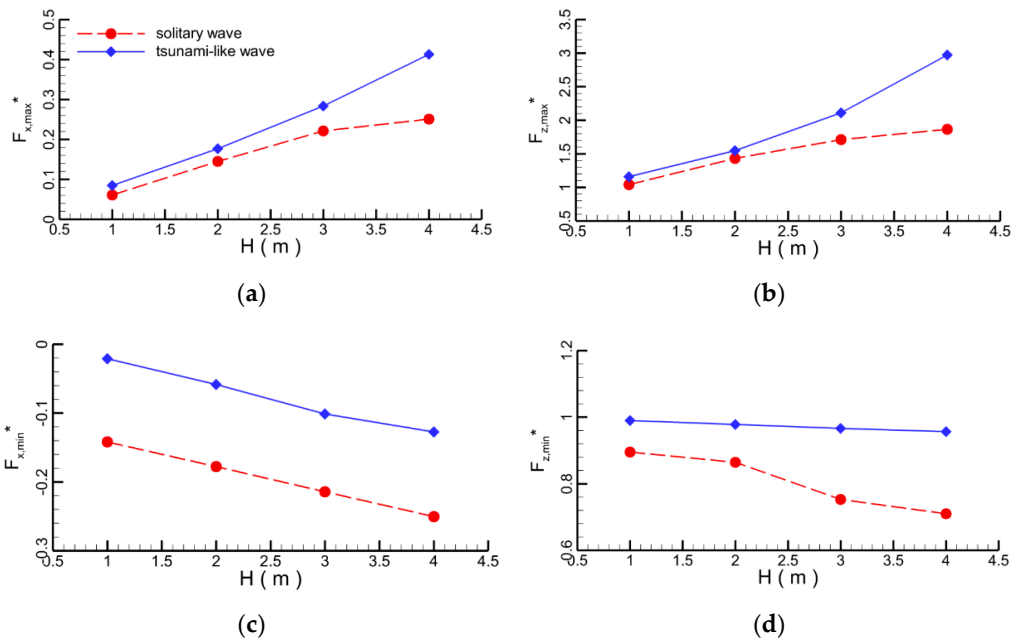


Figure 22. Plots of maximum hydrodynamic forces at the pipeline as a function of wave height; (a) maximum horizontal force  $F_{x,max}^*$ ; (b) maximum vertical force  $F_{z,max}^*$ ; (c) minimum horizontal force  $F_{x,min}^*$ ; (d) minimum vertical force  $F_{z,min}^*$ .

#### 4.1.3. Effect of Pipe Diameter

In ocean engineering, there are submarine pipelines with different diameters. The effects of pipeline diameter on the hydrodynamic forces of tsunami-like waves are analyzed in this section. In the computation, the water depth  $h$  is 10 m, wave height  $H$  is 2 m, and  $G = 0$ . Four different pipeline diameters are selected: 0.8 m, 1 m, 1.2 m, and 1.4 m. When the crest of tsunami-like wave is above the pipeline, the velocity contour of flow field around pipeline is shown in Figure 23. The larger the pipeline diameter, the more serious the impact of the pipeline on the surrounding flow. Under the same tsunami-like wave, the vortex behind the pipeline increases with the increase of the pipe diameter, and the high velocity region around pipeline increases too.

The maximum horizontal and vertical force functions of pipeline diameter are evaluated for the tsunami-like and solitary wave cases (Figure 24). In the figure,  $\beta$  is the ratio of pipeline diameter to the water depth. The maximums of the horizontal and vertical forces increase continuously with pipeline diameter. Meanwhile, at the same wave height, the maximum forces at the pipeline under the tsunami-like wave are always larger than under the solitary wave. It is also observed that the magnitude of the minimum of horizontal force increases as pipeline diameter increases, Figure 24c. However, the magnitude of the minimum vertical force decreases as pipeline diameter increases, Figure 24d.



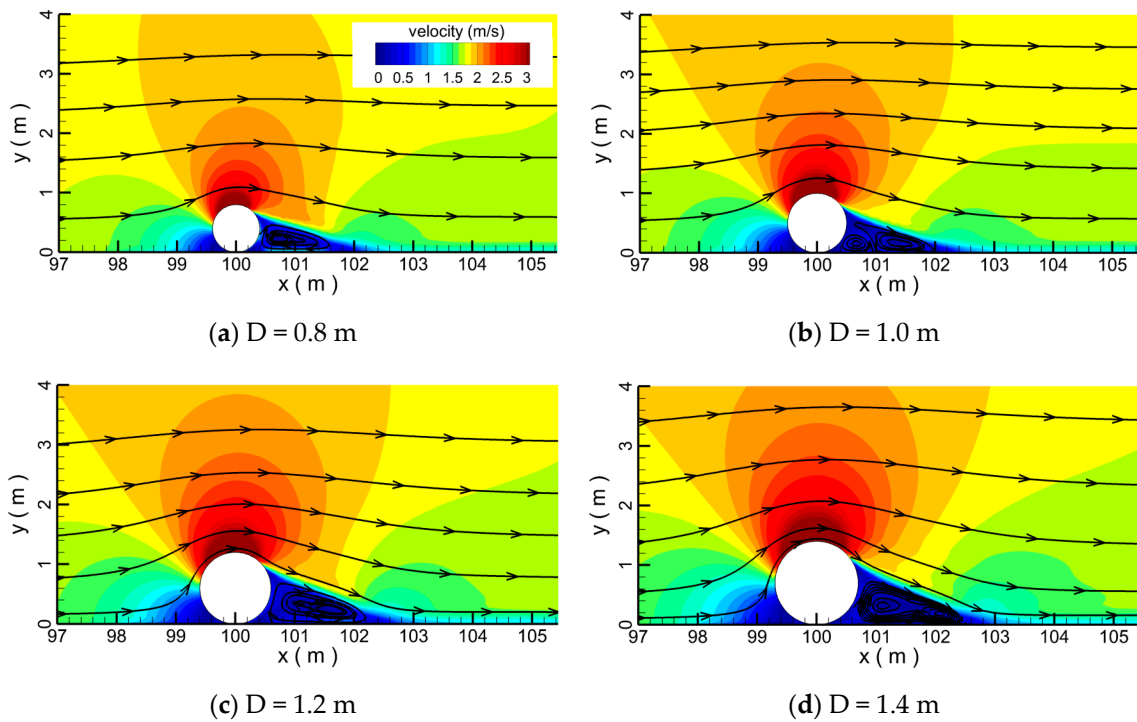


Figure 23. The velocity contours of flow fields around different size pipelines.

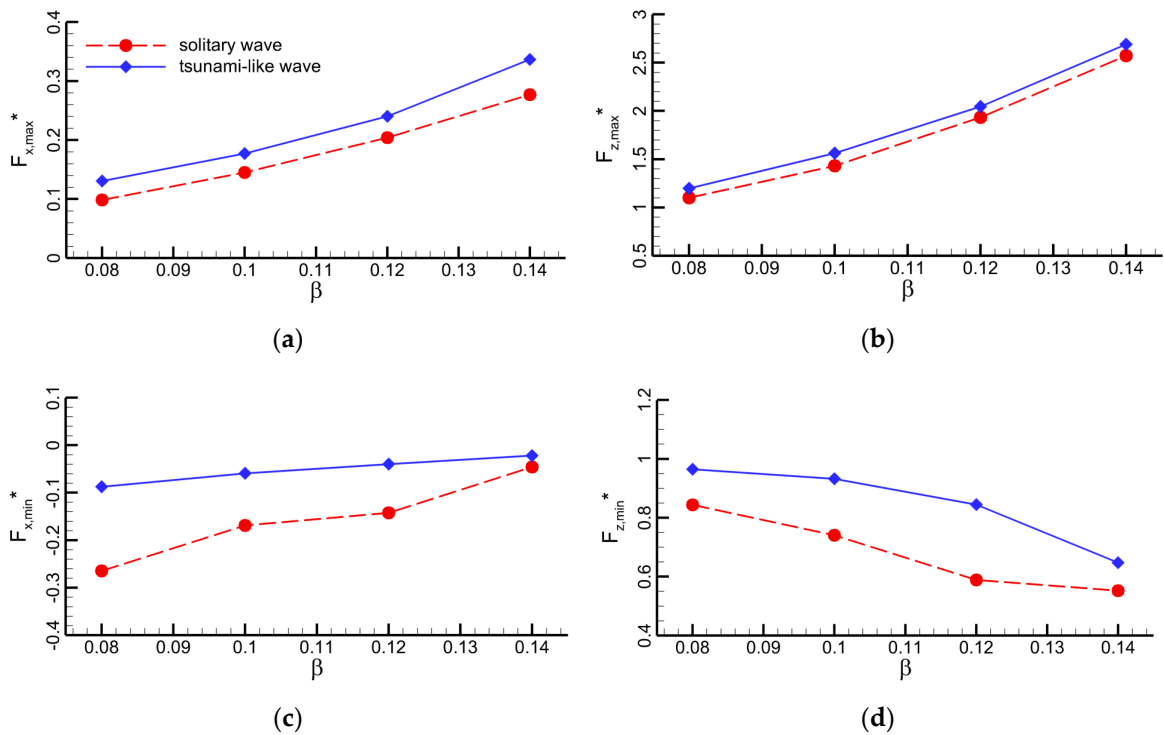


Figure 24. Plots of the maximum horizontal and vertical forces as function of pipeline diameter; (a) maximum horizontal force  $F_{x,max}^*$ ; (b) maximum vertical force  $F_{z,max}^*$ ; (c) minimum horizontal force  $F_{x,min}^*$ ; (d) minimum vertical force  $F_{z,min}^*$ .

#### 4.1.4. Effect of Gap-Ratio

Due to the irregular bathymetry distribution of the seabed, the submarine pipeline can have different clearance heights from the seabed. In this section, the hydrodynamic forces acting on the

suspended pipelines under the tsunami-like wave are numerically analyzed with water depth  $h = 10$  m, and wave height  $H = 2$  m. The ratio ( $\chi = G/D$ ) of the gap between the pipeline and seabed to the pipeline diameter is set as 0.25, 0.5, 0.75, and 1, respectively. Figure 25 plots the snapshots of vortices contour for pipelines with different gap-ratios at  $t = 135$  s under a tsunami-like wave. When the pipeline is close to the seabed, the shedding vortices from the pipeline can have a strong interaction with the seabed boundary layer (Figure 25a). As the gap-ratio increases, the intensity of this kind of interaction gradually decreases, and detached vortices are observed, Figure 25b–d.

The temporal evolution of hydrodynamic forces at the pipeline when the gap-ratio equals 0.25 is shown in Figure 26. It can be seen that the magnitudes of the horizontal and vertical forces are larger for the tsunami-like wave. The tsunami-like wave also has a much longer duration.

The maxima and minima of the horizontal and vertical forces at pipeline as function of gap-ratio are plotted in Figure 27. As the gap ratio increases, the maximum horizontal force gradually decreases, but the rate decreases at same time. This is due to the fact that an increasing gap-ratio will substantially reduce the pressure gradient between the frontal and rear side of the pipeline, resulting in a smaller maximum horizontal force. At the same gap ratio, the maximum horizontal force for the tsunami-like wave is greater than that of solitary wave. Even if the increase of gap-ratio can reduce the pressure gradient, the velocity of the tsunami-like wave is larger than that of a solitary wave. The larger the velocity, the larger the pressure on the pipeline. So, the pressure on the pipeline under the solitary wave is lower than that under the tsunami-like wave. As the gap ratio increases, the maximum vertical force decreases at a much higher rate than the maximum horizontal force. In contrast to the maximum horizontal force, the maximum vertical force for the solitary wave is greater than that of tsunami-like wave for the same gap ratio. The magnitudes of the minimum horizontal and vertical forces gradually decrease with decreasing gap-ratio (Figure 27c,d). The water reflux causes the minimum forces on the submarine pipeline. However, due to the gap exists below the pipeline, much more reflux water can flow through the gap, which reduces the pressure gradient around the submarine pipeline. The reflux velocity above the submarine pipeline under the tsunami-like wave is larger than that under the solitary wave. Depending on the Bernoulli equation theory, the larger the velocity above the submarine pipeline, the lower the pressure above the pipeline. So, the maximum forces under the tsunami-like wave are larger than that under a solitary wave, as shown in Figure 27d.

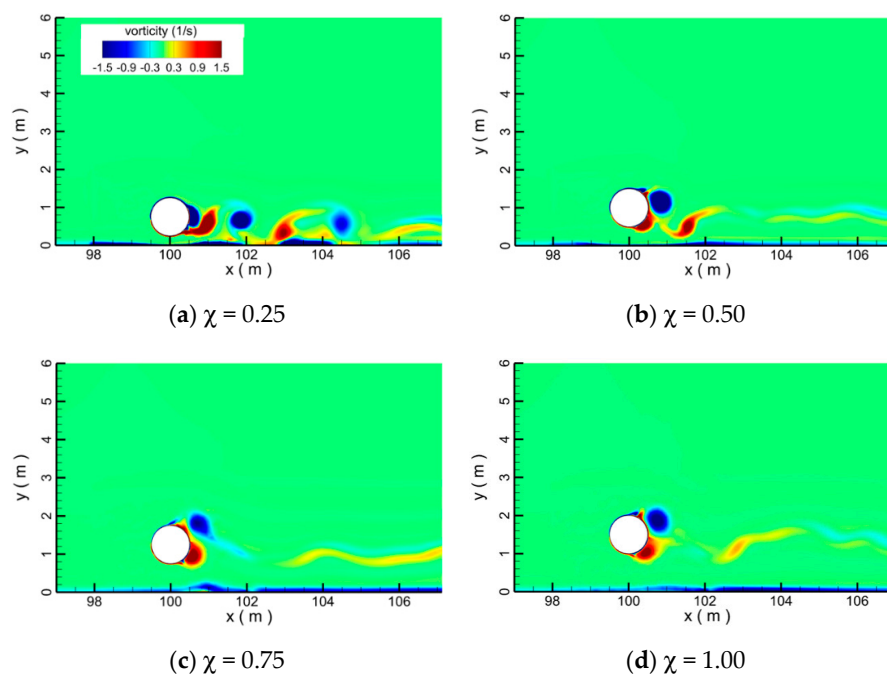


**Figure 25.** Snapshots of vortices contours for pipelines with different gap-ratios at  $t = 135$  s under the tsunami-like wave.

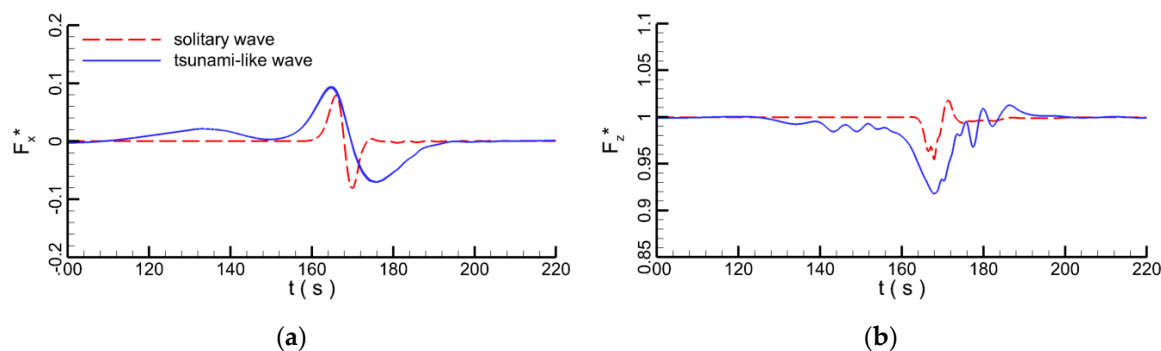


**Figure 26.** Temporal evolution of hydrodynamic forces at a pipeline when the gap-ratio equals 0.25; (a) horizontal force  $F_x^*$  (b) vertical force  $F_z^*$ .

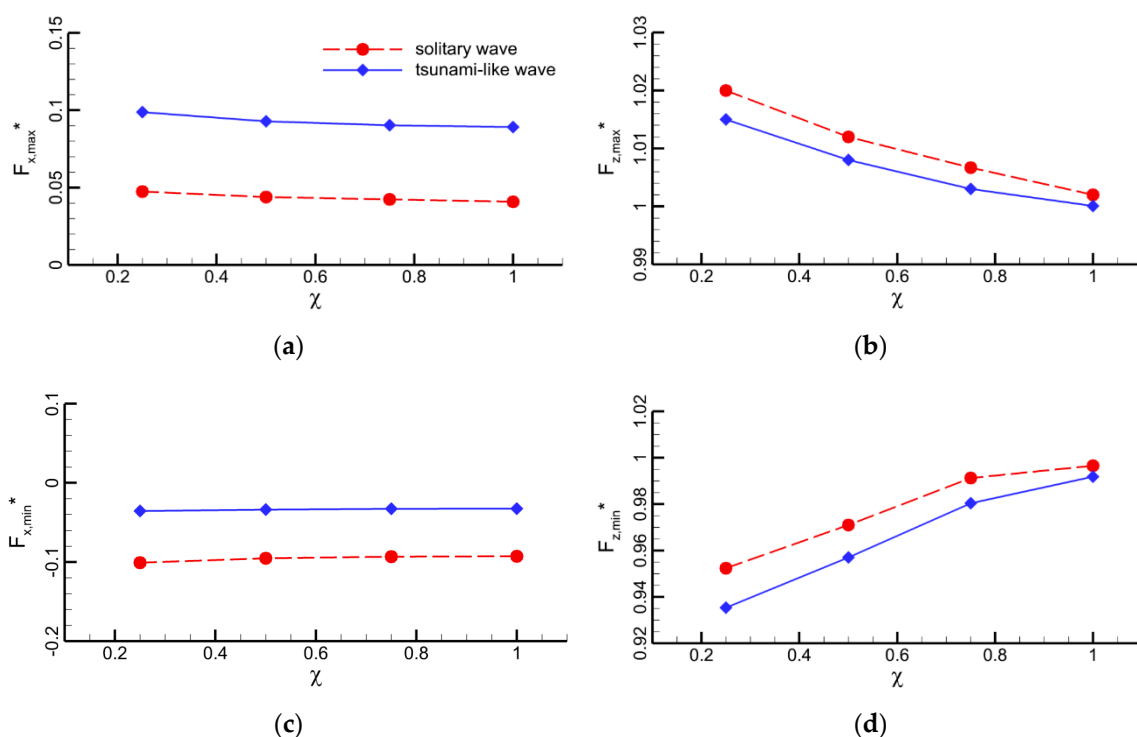


**Figure 27.** Plots of the maximum horizontal and vertical forces as a function of gap-ratio; (a) maximum horizontal force  $F_{x,max}^*$ ; (b) maximum vertical force  $F_{z,max}^*$ ; (c) minimum horizontal force  $F_{x,min}^*$ ; (d) minimum vertical force  $F_{z,min}^*$ .

#### 4.2. Pipelines in Tandem Arrangement

In this section, hydrodynamic characteristics of pipelines in tandem arrangement subjected to a tsunami-like wave are numerically investigated. The corresponding water depth  $h$  and wave height  $H$  in the computation are 10 m and 2 m, respectively. Six different spacing distances are selected: 0.5D, 1D, 1.5D, 2D, 2.5D, and 3D, respectively. The diameter  $D$  of the pipelines is 1 m, and the pipelines are located at  $G = D$  above the seabed.

Figure 28 shows the snapshots of the vortices around the pipelines with different spacing distances for the tsunami-like wave. At 180 s, the vortices behind the single pipeline shed weakly (Figure 28a). When the spacing distance is 0.5 D, the shed vortices from the upstream cylinder directly interact with the boundary layer of downstream cylinder, generating a vortex street with a wide displacement in the vertical direction (Figure 28b). When the spacing distance is D, the intensity of the interaction between pipelines decreases, and a series of shedding vortices in a regular pattern is observed, Figure 28c. If the spacing distance between pipelines is further increased, it is found that vortices shedding

processes are suppressed for both upstream and downstream pipelines due to their mutual interaction, Figure 28d,e. When the spacing distance is 3 D, the vortices shedding process nearly disappears, Figure 28f. The results shown above show that the spacing distances between pipelines have significant influences on their own hydrodynamic characteristics under the impact of a tsunami-like wave.

Compared with a tsunami-like wave (Figure 28), the intensity of vortices shedding processes under the solitary wave is much weaker (Figure 29). When the spacing distance between pipelines is 0.5 D, vortices are disturbed and in disarray (Figure 29b). When the spacing distance between pipelines is larger than 1 D, the influence of upstream vortices on downstream vortices is rather weak (Figure 29c–f).

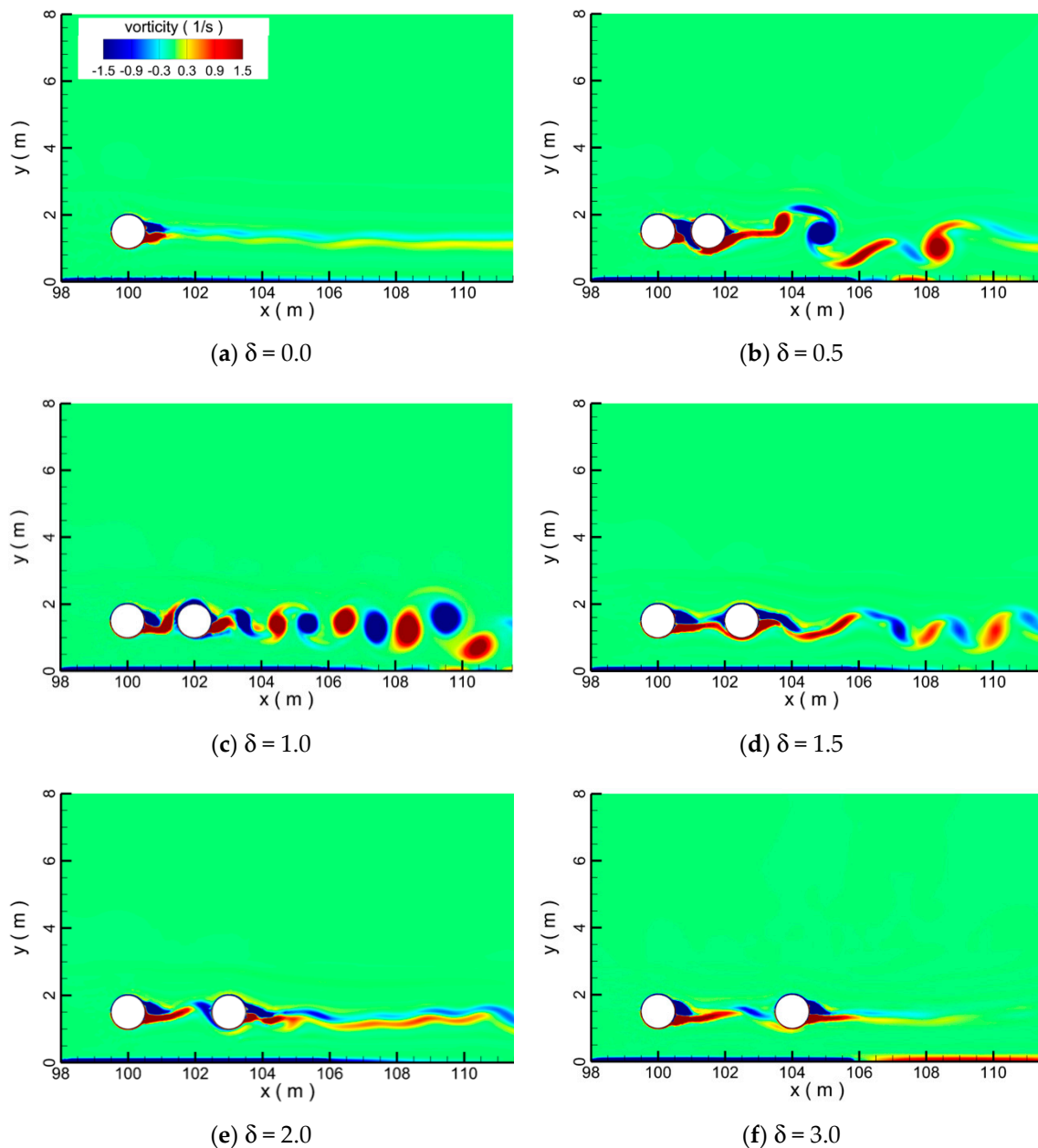


**Figure 28.** Snapshots of vortices contours around a tandem pipeline subjected to a tsunami-like wave at different pipeline spacing distances and  $t = 180$  s.  $\delta$  is the ratio of the distance between the two pipes to the pipeline diameter.

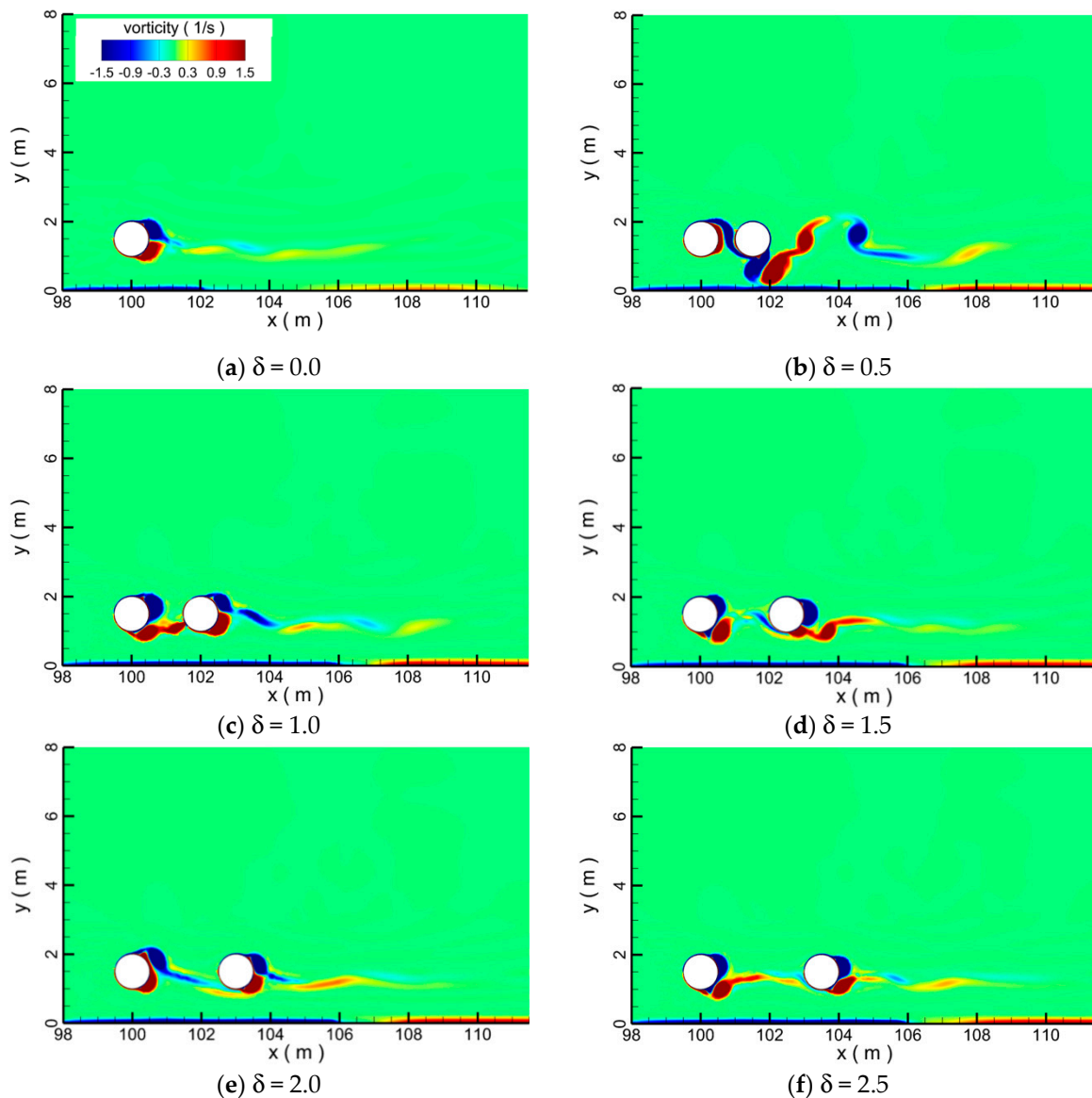
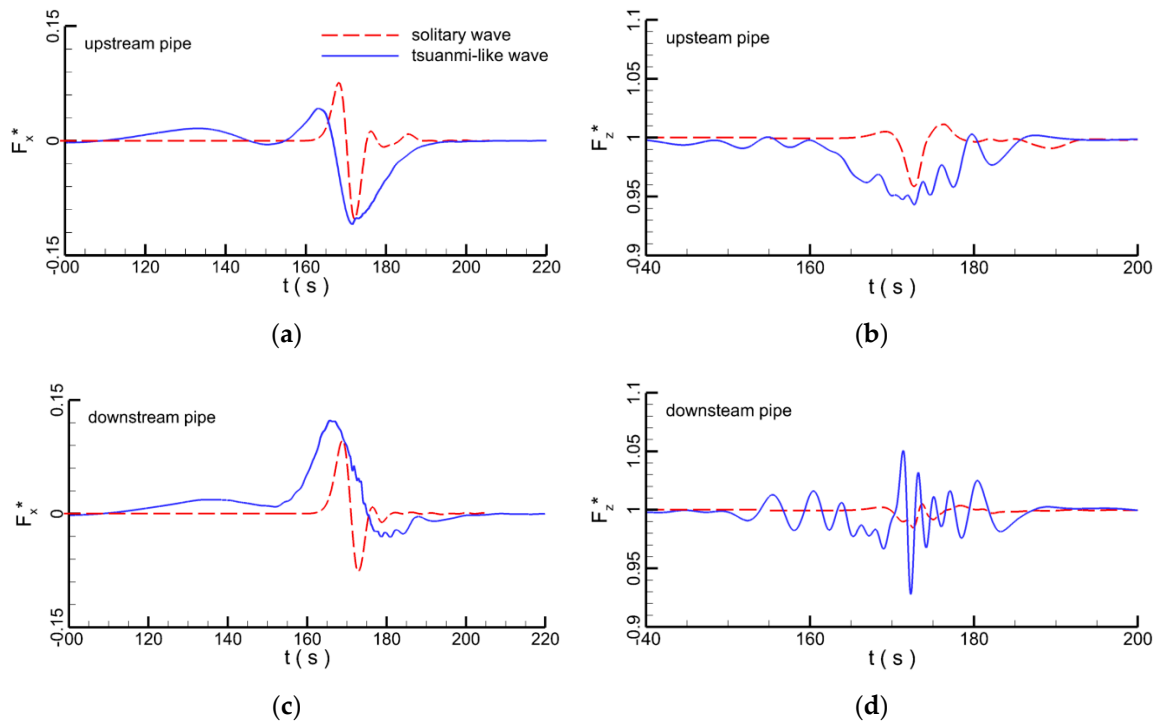


Figure 29. Same as Figure 28 but for a solitary wave at  $t = 22$  s.

The temporal evolutions of the hydrodynamic forces for the tandem pipeline spaced at distance  $1 D$  are plotted in Figure 30 for the solitary and tsunami-like wave cases. Comparing Figure 30a with c, the maximum horizontal peak force is greater for the downstream pipeline for both wave types. The magnitude of the horizontal forces is greater for the tsunami-like wave. The vertical forces of pipelines under the tsunami-like wave exhibit a larger oscillating pattern (Figure 30b,d). The vertical force amplitude is also much greater for the tsunami-like wave.

Figures 31 and 32 depict the maximum and minimum horizontal and vertical forces as a function of the spacing ratio for the pipelines. The maximum horizontal force of the upstream pipeline increases as the spacing distance increases (Figures 31a and 32a). Nonetheless, the maximum horizontal force of downstream pipeline decreases. The horizontal force becomes nearly constant beyond a spacing distance greater than  $2 D$  (Figures 31a,c and 32a,c). The solitary wave also produces a greater maximum horizontal force for the upstream pipeline and a smaller maximum horizontal force for downstream pipeline, compared to the tsunami-like wave. The maximum vertical force on the upstream pipeline decreases almost linearly with the increase of spacing distance (Figure 31b). The tsunami-like wave produces a greater maximum vertical force for both pipelines than the solitary wave (Figures 31b and 32b).



**Figure 30.** Temporal evolution of the hydrodynamic forces at pipelines with spacing distance 1 D under the impact of solitary and tsunami-like waves; (a) horizontal force of upstream pipe  $F_x^*$ ; (b) vertical force of upstream pipe  $F_z^*$ ; (c) horizontal force of downstream pipe  $F_x^*$ ; (d) vertical force of downstream pipe  $F_z^*$ .

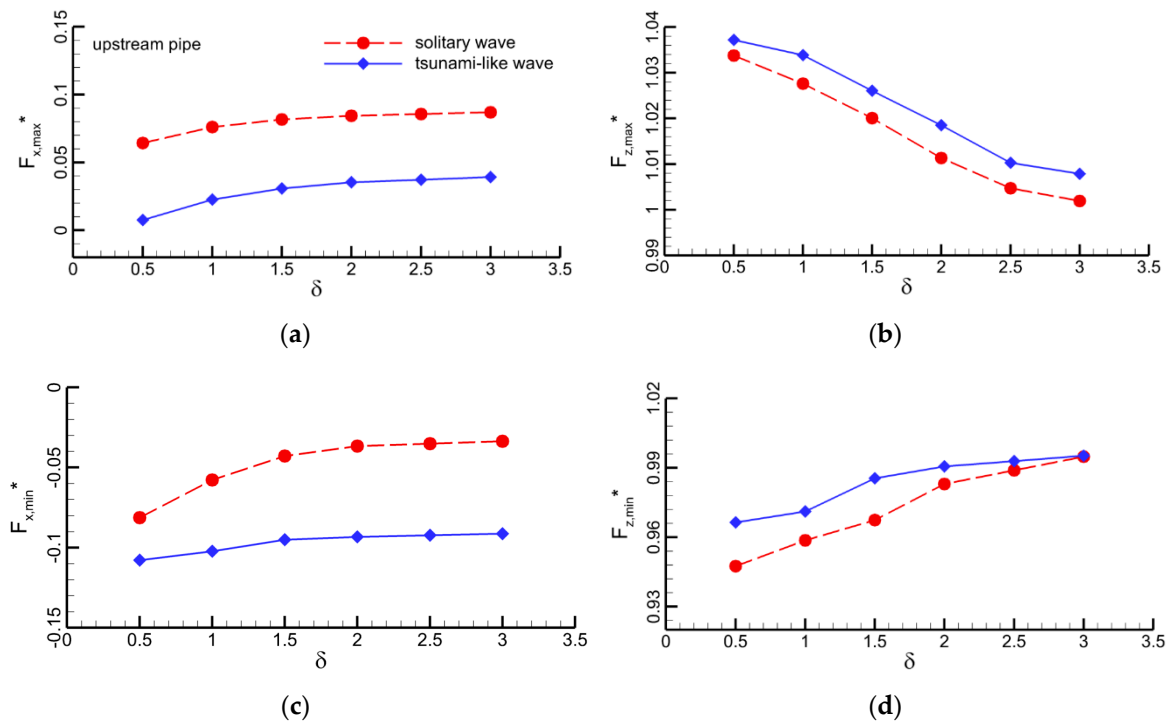


**Figure 31.** Horizontal and vertical forces on the upstream pipeline as function of spacing ratio; (a) maximum horizontal force  $F_{x,max}^*$ ; (b) maximum vertical force  $F_{z,max}^*$ ; (c) minimum horizontal force  $F_{x,min}^*$ ; (d) minimum vertical force  $F_{z,min}^*$ .

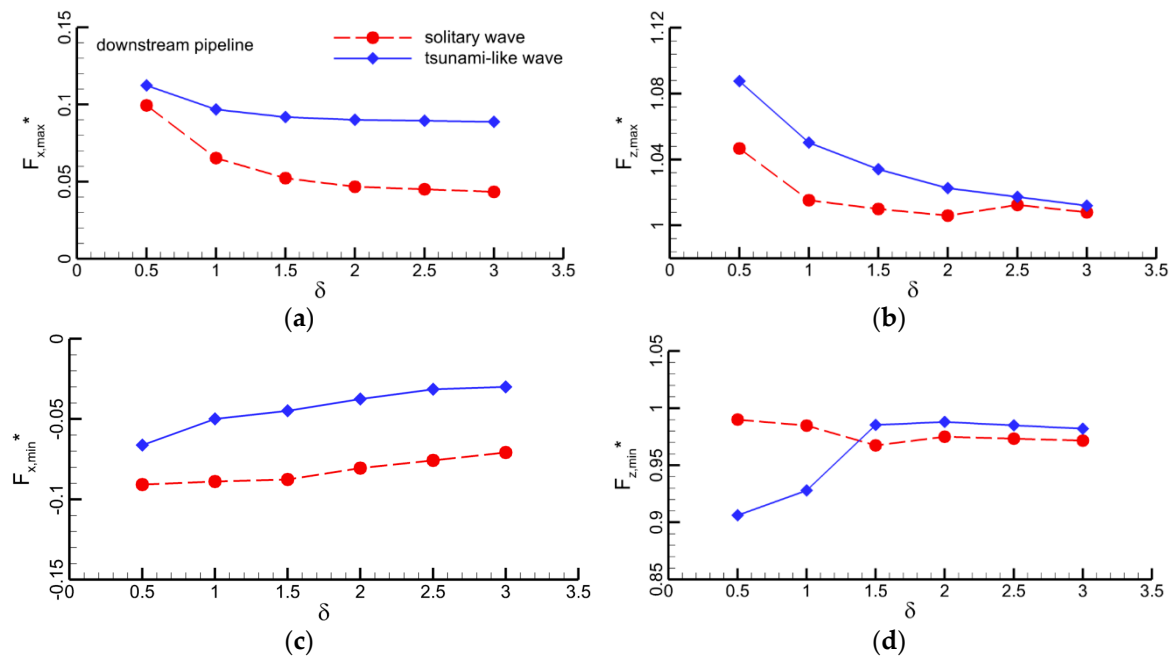


**Figure 32.** Horizontal and vertical forces on the downstream pipeline as function of spacing ratio; (a) maximum horizontal force  $F_{x,max}^*$ ; (b) maximum vertical force  $F_{z,max}^*$ ; (c) minimum horizontal force  $F_{x,min}^*$ ; (d) minimum vertical force  $F_{z,min}^*$ .

## 5. Conclusions

This paper numerically investigates the hydrodynamic characteristics of submarine pipelines impacted by (a) a solitary wave and (b) a more realistic tsunami wave based on N-wave theory. The results strongly depend on which wave model is used. The hydrodynamic characteristics of the tsunami-like wave are drastically different from that of the solitary wave with respect to the structure of flows, force time series, water elevation, and velocity. After the tsunami-like wave has passed the pipeline, the size of the vortices at the frontal and rear sides of pipeline increases substantially. The water free surface under the tsunami-like wave is gentler than under the solitary wave, because the period of the tsunami-like wave is longer than that of the solitary wave. After the solitary wave has passed the pipeline, the vortices behind the pipeline are much smaller than for the tsunami-like wave. When they pass through the pipeline, wave heights decrease for both waves. The wave height of the solitary wave decreases by more than that of the tsunami-like wave. For the tsunami-like wave, the vortex behind the pipeline increases with the increase of pipe diameter. It is also found that hydrodynamic forces at submarine pipelines also may strongly depend on wave height, water depth, pipeline diameter, and gap-ratio. Maximum forces increased with wave height and pipeline diameter. However, the maximum horizontal force decreases with increasing water depth and distance between pipeline and seabed. For the same wave height, the duration of the acting force is much longer for the tsunami-like wave. Overall, the hydrodynamic forces experienced by submarine pipelines are relatively greater when the tsunami-like wave model is used.

The hydrodynamic forces acting on pipelines in tandem arrangement were also discussed. The spacing distance between upstream and downstream pipelines has a significant influence on the forces of the tandem pipeline and the flow field. When the spacing distance is  $0.5 D$ , the shed vortices from the upstream cylinder directly interact with the boundary layer of the downstream cylinder, generating a vortex with wide displacement in the vertical direction. When the spacing distance is  $D$ , the intensity of the interaction between the pipelines decreases significantly, and a series of shedding vortices in a regular pattern is observed. With increasing spacing distance, the maximum horizontal (vertical) forces decreased (increased) continuously at both pipelines. The horizontal forces became nearly constant when the spacing distance exceeds  $2 D$ . All of the discussion presented above supports

the idea that modelling real tsunami waves using the solitary wave model is relatively inaccurate, and that improved wave models should be used instead.

In offshore oil fields, the submarine pipelines are laid on seabed with varying topography. In submarine pipeline construction, whether the seabed is smooth (i.e., relatively flat) or uneven (corrugated, with high points and low points) should be considered as the primary physical factor. If the bed is uneven, the pipeline may include free spans with unsupported sections. If an unsupported section is too long, the bending stress exerted onto it (due to its weight or marine factors) may be excessive. Vibrations from current-induced vortices may also induce the destruction of submarine pipelines. Since most submarine pipelines are laid on flat seabed, in this study, flat seabed was considered. If slopes exist on the seabed, the numerical results will be affected to some extent. Once the waves run up along the slope, the characteristics of the wave change significantly and the broken flow causes different effects on the submarine pipeline. In future research, we will study the effect of tsunami-like waves on submarine pipelines laid on sloped seabed.

**Author Contributions:** Conceptualization, E.Z. and K.Q.; Methodology, E.Z. and K.Q.; Validation, E.Z. and K.Q.; Formal Analysis, L.M.; Investigation, E.Z.; Resources, E.Z. and K.Q.; Writing—Original Draft Preparation, E.Z.; Writing—Review & Editing, L.M., K.Q., S.K. and B.S.; Supervision, L.M.; Funding Acquisition, L.M.

**Funding:** This research was funded by the National Key Research and Development Program of China (Grant No. 2017YFC1404700), the National Natural Science Foundation of China (Grant No. 51809021, and 51839002), the Discipline Layout Project for Basic Research of Shenzhen Science and Technology Innovation Committee (Grant No. 20170418), the Guangdong Special Fund Program for Marine Economy Development (Grant No. GDME-2018E001), and the Fundamental Research Funds for the Central Universities, China University of Geosciences (Wuhan) (Grant No. 2018379010).

**Conflicts of Interest:** The authors declare no conflict of interest.

## References

1. Fang, N.; Chen, G.M.; Zhu, H.W.; Meng, H.X. Statistical analysis of leakage accidents of submarine pipeline. *Oil Gas Storage Transp.* **2014**, *33*, 99–103.
2. Tong, F.F.; Cheng, L.; An, H.; Griffiths, T. The hydrodynamic forces on a circular cylinder in proximity to a wall with intermittent contact in steady current. *Ocean Eng.* **2017**, *146*, 424–433. [[CrossRef](#)]
3. Sumer, B.M.; Fredsoe, J.; Gravesen, H.; Bruschi, R. Response of Marine Pipelines in Scour Trenches. *J. Waterway Port Coast. Ocean Eng.* **1989**, *115*, 477–496. [[CrossRef](#)]
4. Zhao, E.J.; Shi, B.; Qu, K.; Dong, W.B.; Zhang, J. Experimental and Numerical Investigation of Local Scour around Submarine Piggyback Pipeline under Steady Currents. *J. Ocean Univ. China* **2018**, *17*, 244–256. [[CrossRef](#)]
5. Subbiah, K.; Cheong, H.F.; Shankar, N.J. Regular and random wave pressures around large diameter submarine pipeline near ocean bed. *J. Hydraul. Res.* **1991**, *29*, 49–66. [[CrossRef](#)]
6. Gao, F.P.; Gu, X.Y.; Jeng, D.S.; Teo, H.T. An experimental study for wave-induced instability of pipelines: The breakout of pipelines. *Appl. Ocean Res.* **2002**, *24*, 83–90. [[CrossRef](#)]
7. Haley, J.F.; Swan, C.; Gibson, R. An Experimental Investigation of Wave Impact Loads on a Slender Horizontal Cylinder. In Proceedings of the ASME 2014 33rd International Conference on Ocean, Offshore and Arctic Engineering, San Francisco, CA, USA, 8–13 June 2014; American Society of Mechanical Engineers: New York, NY, USA, 2014; p. V08BT06A041.
8. Gao, N.; Yang, J.; Li, X.; Zhao, W. Wave forces on horizontal cylinder due to nonlinear focused wave groups. In Proceedings of the Twenty-fifth International Ocean and Polar Engineering Conference, Kona, HI, USA, 21–26 June 2015; International Society of Offshore and Polar Engineers: Houston, TX, USA, 2015.
9. Chern, M.-J.; Odhiambo, E.A.; Horng, T.-L.; Borthwick, A.G.L. Numerical simulation of vibration of horizontal cylinder induced by progressive waves. *Fluid Dyn. Res.* **2016**, *48*, 015508. [[CrossRef](#)]
10. Ong, M.C.; Kamath, A.; Bihs, H.; Afzal, M.S. Numerical simulation of free-surface waves past two semi-submerged horizontal circular cylinders in tandem. *Mar. Struct.* **2017**, *52*, 1–14. [[CrossRef](#)]
11. Liang, D.F.; Gotoh, H.; Khayyer, A.; Chen, J.M. Boussinesq modelling of solitary wave and N-wave runup on coast. *Appl. Ocean Res.* **2013**, *42*, 144–154. [[CrossRef](#)]



12. Hsiao, S.C.; Lin, T.C. Tsunami-like solitary waves impinging and overtopping an impermeable seawall: Experiment and RANS modeling. *Coast. Eng.* **2010**, *57*, 1–18. [[CrossRef](#)]
13. Limura, K.; Norio, T. Numerical simulation estimating effects of tree density distribution in coastal forest on tsunami mitigation. *Ocean Eng.* **2012**, *54*, 223–232.
14. Synolakis, C.E. The run-up of solitary waves. *J. Fluid Mech.* **1987**, *185*, 523–545. [[CrossRef](#)]
15. Gedik, N.; Irtem, E.; Kabdasli, S. Laboratory investigation on tsunami run-up. *Ocean Eng.* **2005**, *32*, 513–528. [[CrossRef](#)]
16. Goseberg, N.; Wurpts, A.; Schlurmann, T. Laboratory-scale generation of tsunami and long waves. *Coast. Eng.* **2013**, *79*, 57–74. [[CrossRef](#)]
17. Francesco, A.; Tripepi, G.; Meringolo, D.D.; Veltri, P. Solitary wave-induced forces on horizontal circular cylinders: Laboratory experiments and SPH simulations. *Coast. Eng.* **2017**, *129*, 17–35.
18. Madsen, A.; Schäffer, H.A. Analytical solutions for tsunami run-up on a plane beach: Single waves, N-waves and transient waves. *J. Fluid Mech.* **2010**, *645*, 27–57. [[CrossRef](#)]
19. Madsen, A.; Fuhrman, D.R.; Schäffer, H.A. On the solitary wave paradigm for tsunamis. *J. Geophys. Res.* **2008**, *113*, 286–292. [[CrossRef](#)]
20. Chan, I.C.; Liu, L.F. On the run-up of long waves on a plane beach. *J. Geophys. Res.* **2012**, *117*, 72–82. [[CrossRef](#)]
21. Qu, K.; Ren, X.Y.; Kraatz, S. Numerical investigation of tsunami-like wave hydrodynamic characteristics and its comparison with solitary wave. *Appl. Ocean Res.* **2017**, *63*, 36–48. [[CrossRef](#)]
22. Stefan, L.; Oumeraci, H. Solitary waves and bores passing three cylinders-effect of distance and arrangement. *Coast. Eng. Proc.* **2014**, *1*, 39.
23. Istrati, D.; Buckle, I.; Lomonaco, P.; Yim, S. Deciphering the Tsunami Wave Impact and Associated Connection Forces in Open-Girder Coastal Bridges. *J. Mar. Sci. Eng.* **2018**, *6*, 148. [[CrossRef](#)]
24. Zhao, E.J.; Mu, L.; Shi, B. Numerical Study of the Influence of Tidal Current on Submarine Pipeline Based on the SIFOM–FVCOM Coupling Model. *Water* **2018**, *10*, 1814. [[CrossRef](#)]
25. Rhie, T.M.; Chow, A. Numerical study of the turbulent flow past an isolated airfoil with trailing-edge separation. *AIAA J.* **1983**, *21*, 1525–1532. [[CrossRef](#)]
26. Gomes, M.N.; Olinto, C.R.; Rochaa, L.A.O.; Souzaa, J.A.; Isoldi, L.A. Computational modeling of a regular wave tank. *Therm. Eng.* **2009**, *8*, 44–50.
27. Hafsia, Z.; Haj, M.B.; Lamloumi, H.; Maalel, K. Comparison between Moving Paddle and Mass Source Methods for Solitary Wave Generation and Propagation over A Steep Sloping Beach. *Eng. Appl. Comput. Fluid Mech.* **2009**, *3*, 355–368. [[CrossRef](#)]
28. Qu, K.; Ren, X.Y.; Kraatz, S.; Zhao, E.J. Numerical analysis of tsunami-like wave impact on horizontal cylinders. *Ocean Eng.* **2017**, *145*, 316–333. [[CrossRef](#)]
29. Sibley, P.O. The Solitary Wave and the Forces It Imposes on a Submerged Horizontal Circular Cylinder: An Analytical and Experimental Study. Ph.D. Thesis, City University London, London, UK, 1991.

